NASA-TM-79181 19790023093

NASA Technical Memorandum 79181

LIFE CHARACTERISTICS ASSESSMENT OF THE COMMUNICATIONS TECHNOLOGY SATELLITE TRANSMITTER EXPERIMENT PACKAGE

Jerry Smetana and Arthur N. Curren
Lewis Research Center
Cleveland, Ohio

July 1979

SUMMARY

The performance characteristics of the transmitter experiment package (TEP) aboard the Communications Technology Satellite (CTS) measured during its first 2 years in orbit are presented in this report. The TEP consists of a nominal 200-watt output stage tube (OST), a supporting power processing system (PPS), and a variable-conductance heat pipe system (VCHPS). The OST, a traveling-wave tube augmented with a 10-stage depressed collector, has an overall saturated average efficiency of 51.5 percent and an average saturated radiofrequency (rf) output power at center-band frequency of 240 watts. The PPS operated with a measured efficiency of 86.5 to 88.5 percent. The VCHPS, using three pipes to conduct heat from the PPS and the body of the OST to a 52- by 124-centimeter (20.5- by 48.75-in.) radiator fin, maintained the PPS baseplate temperature below 50° C for all operating conditions. The TEP performance characteristics presented include frequency response, rf output power, thermal performance, efficiency, and distortions. Communications characteristics were evaluated by using both video and audio modulated signals. The results are as follows:

1. Operation of a high-voltage (11.2 kV), high-power (570 W) electrical system has been demonstrated.

2. The TEP supports all CTS video and audio applications and provides high-quality communications.

3. An OST operating efficiency greater than 50 percent and a saturated rf output power greater than 200 watts were achieved.

4. There were no observable degradations in TEP performance due to launch, preinjection, and operating environments or due to 2 years of in-orbit operation.

On four occasions, the TEP experienced temporary thermal control system malfunctions. While each of the anomalies was terminated safely, an investigation of the problem was conducted because of the potential for TEP damage due to the significant temperature increases associated with the anomalies. The investigation revealed the probable cause of the anomalies and safe TEP operating procedures have been established and are being observed.

INTRODUCTION

The Communications Technology Satellite (CTS) was developed jointly by NASA and the Canadian Department of Communications. It was launched from Cape Kennedy on January 17, 1976, and later placed in an equatorial geostationary orbit at 116° west longitude, just west of South America, at an altitude of about 35 887 kilometers

(22 300 miles). From this position, CTS broadcasts in a newly-allocated satellite frequency band (12 GHz) to Canada and the United States, including Alaska. New technology has increased the CTS transmitting power level up to 20 times that of earlier satellites, permitting television reception and two-way voice communication with relatively inexpensive ground equipment in the areas served. The satellite is being used to demonstrate new technology and to conduct communication experiments that are concerned with satisfying the needs of various segments of society. The communications experiments include programming related to technology, education, medicine, business, emergency services, and radio and television services.

A salient characteristic of the CTS spacecraft that distinguishes it from prior communications satellites is its rf output transmitter power. It has simultaneous transmitter outputs of 20 and 200 watts. It uses two 85-megahertz bands centered at 14.052 and 14.247 gigahertz for uplink transmissions. These signals are translated to two 85-megahertz bands centered at 11.885 and 12.080 gigahertz and retransmitted to earth with rf output powers of up to 20 and 200 watts, respectively. Its maximum rf output power of 200 watts is an order of magnitude greater than that of earlier communications satellites. This high rf output power is developed in the 85-megahertz frequency band at 12.080 gigahertz by the transmitter experiment package (TEP).

The TEP (ref. 1) consists of a nominal 200-watt output stage tube (OST), a supporting power processing system (PPS), and a variable-conductance heat pipe system (VCHPS). The OST is a coupled-cavity, traveling-wave tube augmented with a multistage depressed collector. The PPS supports the operation of the OST by providing control for remote-command operation as well as protection and regulated operating voltages. The VCHPS is used to remove heat from the body of the OST and from the PPS.

Unique design approaches were used in achieving high efficiency - specifically, velocity tapering of the output coupled-cavity, slow-wave structure to achieve an interaction efficiency of 26 percent; a nine-active-stage (plus one at ground potential) multi-stage depressed collector (MDC) with beam refocusing to achieve a collector efficiency of 82 percent; and samarium cobalt magnets for output section focusing. In-flight, these design approaches produced an OST average overall efficiency of 51.5 percent at an average saturated rf output power of 240 watts at center-band frequency. A two-stage regulator composed of a switching chopper preregulator and a paralleled inverter for voltage scaling led to a dc-dc PPS efficiency of 86.5 to 88.5 percent. Stringent requirements were met for low output ripple, high regulation, and low stored energy.

The design approach selected for thermal control of the OST collectors was to use direct radiation from the MDC enclosure, which operates with a maximum in-orbit temperature of 180° C. A VCHPS composed of three pipes and a 52-centimeter by 127-centimeter fin radiator maintained OST body temperatures between 35° and 60° C. This was accomplished for in-orbit operating conditions that resulted in heat rejection rates of 20 to 180 watts.

The results of testing during the first 90 days of TEP operation are detailed in reference 2. This present report presents test results obtained from in-orbit tests conducted to monitor and evaluate on a continuing basis the rf, electrical, and thermal performance of the TEP. The period covered by this report consists of the first 2 years of on-orbit operation, specifically from February 8, 1976 to February 8, 1978. During that 2-year period, the TEP accumulated 9150 hours of operation. Prior to launch, the TEP was also operated for 1800 hours in ground testing.

In-orbit operating test results are presented for the OST, PPS, and VCHPS. Thermal in-orbit performance is presented for the OST, MDC, and VCHPS. In-orbit, the OST and PPS have demonstrated operating efficiencies of 51.5 and 88.5 percent, respectively.

Communications test results for the high-power, high-efficiency TEP are presented. In-orbit saturated power output, frequency, and power transfer characteristics remain unchanged from ground test results. Results obtained by using the TEP for single-channel frequency-modulated (FM) video transmissions demonstrate the TEP's continuing capability to support the CTS communications applications with low-cost ground terminals.

The losses attendant on the large power consumption of the TEP necessitated special test techniques to accommodate widely varying heat rejection rates from both the OST body and the directly radiating MDC enclosure. Because the operating thermal environment is influenced greatly by its operating point, it was necessary for test purposes to operate the TEP at constant rf power levels to achieve thermal equilibrium. This was done to establish repeatable test conditions. The thermal performance and effects are discussed in this report.

DESCRIPTION OF EQUIPMENT

CTS TRANSPONDER

The CTS super-high-frequency (SHF) transponder system provides two wide-band microwave downlink channels in the 12-gigahertz frequency band. The rf amplifiers used in both channels are 20 and 200 W traveling-wave tubes (TWT). The higher

power channel uses an advanced technology TWT with a multistage depressed collector (MDC), which contributes to the tube's high-efficiency operation.

The CTS SHF transponder consists of the following major elements

(1) Two receivers (one backup)

(2) Two low-power TWT driver amplifiers (one backup)

(3) Two dual purpose receiving and transmitting antennas

(4) A switching and filtering system

(5) A high-power and high-efficiency microwave amplifier

(6) A power conditioning system

(7) A SHF beacon system

A block diagram of the major components of the SHF transponder is shown in figure 1. The frequency plan is presented in figure 2. The SHF transponder can simultaneously process signals in either of its two 85-megahertz-wide bands. A signal transmitted to the spacecraft in receive band 2 (RB2)(see fig. 2) will be retransmitted to Earth in transmit band 2 (TB2) through the 20-watt TWT driver/amplifier. A signal transmitted to the spacecraft in RB1 will be retransmitted to Earth in TB1 through the 200-watt high-efficiency TWT.

TRANSMITTER EXPERIMENT PACKAGE

A major subassembly of the CTS spacecraft SHF transponder is the transmitter experiment package. This subassembly consists of the following major components: (1) a power processing system, (2) an output stage tube consisting of the 200-watt traveling-wave tube and the multistage depressed collector, and (3) a variable-conductance heat pipe system consisting of the radiator, reservoirs, and three heat pipes. Figure 3 is a diagram showing the layout of the TEP subassembly.

Power Processing System

Two spacecraft power sources supply direct-current (dc) power to the power processing system. These sources are the experiments bus, with a nominal voltage of 76 volts dc, and the housekeeping bus, with a nominal voltage of 27.5 volts dc. The PPS converts the spacecraft voltages to the several voltages needed for the operation of the 200-watt, traveling-wave tube. The PPS voltages and system performance characteristics are shown in table I.

Two voltage protection circuits are incorporated into the PPS in the event of an input over voltage or undervoltage malfunction. Additional circuits cause protective shutdowns because of excess OST body current or internal pressure. In addition, a number of voltage, current, and temperature measurements are interfaced through the PPS to the main spacecraft telemetry system. All telemetry data are encoded by one of two encoders. The data allocation is such that not all the TEP measured parameters are available unless the correct encoder is operating. The TEP telemetry measurement summary is presented in table II. The spacecraft command system is designed to accept 225 commands. The TEP responds to 20 commands whose function is to control the operation of the TEP.

Output Stage Tube

The OST is a coupled-cavity, linear-beam, traveling-wave-tube amplifier (ref. 1). Highly efficient amplifier operation is realized through two major design features. a velocity taper in the slow-wave structure, and an MDC. The velocity taper synchronizes the bunched electron beam with the rf wave moving along the tube body to provide a high level of tube interaction efficiency (25 percent). The 10-plate depressed collector (nine active plates plus one at ground potential) sorts out and reduces the velocities of the spent-beam electrons so that the electrons are collected at near zero velocity, with low kinetic energy. This unique collector (ref. 3) produces efficient conversion of the spent beam kinetic energy to potential energy and lessens the amount of dc power required to operate the TWT.

The OST performance specifications are presented in table III and figure 4 is a photograph of the flight model.

Variable-Conductance Heat Pipe System

The PPS and the OST are mounted on the spacecraft south equipment panel which provides the thermal rejection mainly for the PPS. The VCHPS supplements the OST baseplate thermal rejection capability by providing additional heat transport from the baseplate when needed. Adequate heat rejection can be obtained with one of the three heat pipes failed. The VCHPS mated to the TEP is shown in figure 3.

NASA GROUND STATION

The NASA Lewis Research Center SHF ground-station facility provides the main support for the TEP SHF technology experiment. The main operating requirements

of the facility are: (1) to provide a high-power (85-dBW effective isotropic radiated power (EIRP) wide-band, FM (video and audio) uplink signal to the spacecraft at 14 gigahertz, (2) to provide a low-noise, downlink receiving capability at 12 gigahertz (video and audio), and (3) to provide the capability of displaying video, audio, and telemetry data for real-time evaluation of electrical, thermal and communications parameters of the CTS transponder and TEP The functional block diagram of the facility is shown in figure 5. The facility's characteristics are presented in table IV.

The Lewis ground-station facility consists of three operational elements the transmit-receive terminal, the experiment evaluation center (EEC), and the spacecraft control center (SCC).

Transmit-Receive Terminal

The high-power uplink transmitter consists of two identical low-power modulators, two intermediate driver amplifiers, a two-channel combiner, and a high-power transmitter. Baseband video and audio signals applied to the modulators produce 14-gigahertz FM signals at their outputs. Either one or two FM channels may be processed through the channel combiner. The low-power, FM, video-audio channel is amplified by the intermediate power driver, the output of which is used to excite the high-power klystron. The high-power transmitter system employs two klystrons (type VKU 7791) with a common power supply and common input-output circuitry. Only one klystron may be operated at a time. The characteristics of the klystrons are identical except for frequency. One is tuned for uplink band 1 (RB1); the other is tuned to uplink band 2 (RB2). Both klystrons are air cooled, and the entire transmitter system can be operated remotely from the EEC.

A parametric amplifier (Paramp) or a tunnel diode amplifier (TDA)(switch selectable) are used for pre-amplification of the received signals. The paramp is a recent addition to the system and the TDA is used as a backup. Two 12 gigahertz tunable receivers are used for dual channel operation. The uplink-downlink system has the capability to generate and demodulate video carriers with frequency deviation from 10 to 30 megahertz peak to peak and the system can operate with or without pre-emphasis or de-emphasis. Normally the system is operated at modulation index two (18 MHz p-p) with pre-emphasis and de-emphasis.

The ground terminal antenna system consists of a 5-meter (16-ft) diameter parabolic reflector with a Cassegrain feed, a beacon receiver and a step-track antenna

control. The reflector, feed assembly, and pedestal (elevation over azimuth) mounting structure are mounted on the roof of a building at the Lewis Research Center. The associated tracking, controlling, and monitoring equipment is located in the EEC, which is in another building at Lewis. A step-track system, which is locked to a 11 7 gigahertz spacecraft beacon, can continuously update the antenna-pointing toward the spacecraft with an accuracy of $\pm 0.05^{\circ}$.

Experiment Evaluation Center

The SHF experiment is conducted and evaluated from the EEC. The EEC serves as the main facility for displaying, switching, controlling, and evaluating video, audio, and telemetry data. Both the uplink transmitter and the 5-meter (16-ft) dish antenna can be controlled from this location. All audio and video signals generated in the communications laboratory are routed through the EEC to the modulators. All signals received from the spacecraft are similarly routed through the EEC to various display and recording equipment, which includes two 2 inch video tape recorders.

Spacecraft Control Center

The spacecraft control center is physically located in the same room as the EEC. This facility contains telemetry demodulator, analog magnetic tape recorder, digital magnetic tape recorder, computer, CRT displays and line printers. Its function is to receive telemetry from Goddard Space Flight Center, record the raw data, process the data and display or record real-time (or old) data in engineering units.

GENERAL PROCEDURES

The TEP test and evaluation program was segmented into three phases. Phase I consisted of nine continuous days of testing, 24 hours per day, beginning with the first TEP turn-on, February 8, 1976. The purpose of this phase of testing was to perform initial in-orbit evaluation of TEP performance by comparing prelaunch data with in-orbit data and to verify that the TEP had survived the launch. Phase II testing was performed during two 24-hour days each week for 12 weeks of TEP operation. The TEP was not operated during the eclipse period March 4 to April 23, 1976, so this phase was not completed until June 13, 1976. The purpose of this phase was to characterize the electrical, thermal and communications performance of the TEP. The results of Phases I and II were reported in reference 2.

Phase III, then, continued with testing once each month to evaluate the life characteristics of the TEP. The design life of the TEP was 2 years and, therefore, it is appropriate that an assessment of the life characteristics be reported after 2 years in orbit.

HOW THE TESTS ARE PERFORMED

The tests performed during Phase III were limited to the tests needed to evaluate life performance:

Thermal Stability Test
Frequency Response Test
Power Transfer Characteristics Test
High Voltage Leakage Test
Single Channel Video Test

These tests were performed by transmitting appropriate SHF signals from the ground terminal through the CTS spacecraft, by receiving these signals at the Lewis Research Center (LeRC) and evaluating these signals at the SCC or EEC. The tests require that both antennas on CTS be pointed towards LeRC. The LeRC 5-meter antenna is locked onto the beacon signal and it tracks the spacecraft continuously. For some tests, Frequency Response Test and Power Transfer Characteristics Test, in which the updating of antenna pointing can disturb the measurements, the ground antenna is locked in place for 5 to 10 minute intervals.

HOW THE MEASUREMENTS ARE MADE

Video tests are made by transmitting precisely generated program video/audio or standard National Television System Committee (NTSC) signals and then measuring the received signals. Video measurements are signal-to-noise ratio, differential gain, differential phase and subjective analysis. Audio test-tone-to-noise measurements are also made.

Electrical and thermal data are transmitted from the satellite by its S-band telemetry channel to Communications Research Center (CRC), in Ottawa or to one of NASA's Space Tracking and Data Network (STDN) stations. From the telemetry reception station the data is transmitted by landline through Goddard Space Flight Center to LeRC's SCC. Here the raw data is stored on magnetic tape and processed using an EMR 6130 computer to provide real-time display of CTS performance in engineering units. The transmission and processing delay time for the real-time data is 2 to 6 seconds. The data is displayed on several cathode ray tube monitors

(CRT) in SCC and EEC and on a large visitor's information panel. A thermal copier and a line printer are available to make permanent copies.

Similarly, flag channels are transmitted by telemetry which give the status of dual-state devices on the spacecraft.

In addition, locally generated data is "hard-line" fed to the computer so that relevant ground terminal parameters may be displayed and recorded with the spacecraft data. They are:

Unlink power
Uplink frequency
Ground station received power
Beacon received signal
Spurious signal level
Antenna elevation
Antenna azimuth

In addition to the measured parameters the computer calculates and displays in real-time calculated parameters such as:

Downlink frequency
OST forward output power (S/C detector)
OST reflected power
Spacecraft received signal
Transponder gain
OST beam transmission efficiency
OST interaction efficiency
OST total efficiency
OST DC input power
Sum of OST collector currents
Experiments (76-V) array power
Housekeeping (27.5-V) array power
OST output power (DC derived)
Beacon signal variation
Ground derived OST output power
Ground derived transponder gain
Ground derived interaction efficiency
Ground derived total efficiency

A disc recorder is used to store up 300 samples (at an input rate of one sample per second) of data from 14 channels. Using the disc-recorded data and a plotting routine in the computer the following plots can be displayed on a CRT within a few seconds after the data is stored:

OST output power vs frequency
Body current vs frequency
Beam transmission efficiency vs frequency
Interaction efficiency vs frequency
OST total efficiency vs frequency
Transponder gain vs frequency
Spacecraft received signal vs frequency
Beam current vs frequency
Ground derived OST output power vs frequency
Ground derived interaction efficiency vs frequency
Ground derived OST total efficiency vs frequency
Ground derived transponder gain vs frequency
OST output power vs spacecraft received signal
Ground derived OST output power vs spacecraft received signal
Permanent records of these plots can be made using the thermal copier.

TEST PROCEDURES

In the monthly tests during phase III the regular schedule consists of four thermal stability tests at four quadrant earth orbit positions of the satellite, 0^{o}, 90^{o}, 180^{o}, and 270^{o}, a frequency response test and a power transfer characteristic test. At the beginning of each test day a current sensor offset calibration test is performed wherein the computer stores a data set of telemetry data from all current sensors on the spacecraft with the TEP turned off. This current offset test establishes the zero current intercept of the current vs telemetry counts for each sensor. The slope is assumed to remain as initially calibrated before launch. All telemetry data from the spacecraft has 256 bit resolution, is transmitted at one sample per second and is estimated to be within 1 percent accuracy. The other tests listed earlier in this section are performed once each year.

The thermal stability tests are performed by driving the spacecraft transponder to produce constant OST output for 2 hours. Spacecraft hardline and calculated data are recorded using the line printer at 5-minute intervals. Spacecraft thermal response is analyzed by plotting data from each thermal stability test and thermal effects as a function of time. Spacecraft position, earth/sun relationship or sun angle are analyzed by plotting data from the last printout of appropriate tests.

Frequency response data are obtained by driving the uplink transmitter in leveled mode (within 0.5 dB) across the OST band 14.205 to 14.290 GHz slowly (for 200 sec). The levels are set at centerband to produce saturated output at the OST and 1, 3, 6, and 10 dB below saturated output. Data is recorded by using the plotting routine described earlier.

Power transfer characteristics are generated by overdriving the OST to the point where its output is about 0.5 dB below saturated output and then reducing the drive slowly (during a 200 sec interval) through a 16 dB range. Data is recorded by using the plotting routine. The tests are performed at 5 equally spaced frequencies across the band 14.205, 14.226, 14.247, 14.268, and 14.290 GHz.

Saturated output is defined as the drive power operating point of the OST where a further increase in drive power produces essentially no increase in OST output power. Saturation is achieved by over-driving the OST and then backing off until the output power just begins to decrease.

DISCUSSION OF RESULTS

After the completion of the initial evaluation of TEP performance, phase I (first 9 days) and the characterization of the OST, PPS and Heat Pipe System, phase II (90 days of operation), regular testing of the TEP continued although less frequently to evaluate the life characteristics of the TEP.

This section will present data showing the electrical, thermal and communications characteristics of the OST, PPS and Heat Pipe System during the 2-year period from February 1976 to February 1978. During this time the TEP had been operating (the beam was turned on) 9150 hours which amounts to 52 percent utilization (60 percent actually, because the TEP was shutdown 98 days during 2 eclipse periods). The TEP is turned to standby condition when no user operation is scheduled for 4 hours or more. In addition the TEP accumulated 1800 hours of operating time during prelaunch testing.

ELECTRICAL CHARACTERISTICS

Efficiency

The PPS efficiency is defined as:

$$\eta_{PPS} = \frac{\text{Total DC Power Delivered to the OST}}{\left(\begin{matrix}\text{Total DC Power} \\ \text{Delivered to the PPS}\end{matrix}\right) - \left(\begin{matrix}\text{DC input Power} \\ \text{Used for Instrumentation}\end{matrix}\right)}$$

The power delivered to the OST was obtained by summing the collector power, the anode power, the cathode heater power and the power loss due to electron interception on the rf structure. The input power was taken as the sum of the power from the housekeeping (27.5 V) array and the experiments (76 V) array. Seven watts were used as the power accountable to instrumentation. The OST efficiency is defined:

$$\eta_{OST} = \frac{\text{rf output power}}{\text{Total DC power delivered to the OST}}$$

Figure 6 shows PPS and OST efficiency plotted versus time (days after launch). The PPS efficiency is plotted using data from the saturated rf output power, centerband frequency condition of the thermal stability test which was tested most often. The OST efficiency calculation at that condition was not valid because these efficiencies were computed using the incorrect on-board rf power detector measurement. During the second year of operation this measurement was inconsistent at saturated rf output power. However, at the 100-watt level the on-board rf power detector diode measurements produced consistent results and the OST efficiency calculations are considered to be valid. It can be inferred that, if the efficiency remained constant for 2 years at 100 watts, it did not change at other power levels.

RF Output Power

Figure 7 shows OST rf output power and DC electrical input power plotted versus time (days after launch) for a 2-year period. The rf power measurement used in this plot is an empirically derived power measurement from the DC power inputs to the PPS and OST. It is computed from

$$TPRF = 0.007965\ P_{76} - 149.35 - V_K(I_B - 6)$$

where

P_{76}	DC power delivered to the PPS from the experiments array (76-V bus), W
V_K	cathode voltage, kilovolts
I_B	body current, milliamperes
$(I_B - 6)$	zero for negative values

It became necessary to calculate power levels over 200 watts since the on-board rf detector began operating inconsistently at power levels over 200 watts.

The calculated power values can be shown to be a reliable measure of rf output power if PPS efficiency, OST efficiency, cathode voltage and body current do not change. Table V shows, for the first and second year of operation, the computed mean and standard deviation of the parameters that were assumed to remain unchanged as well as the OST output power and input power. Note that the difference between the first year and second year mean value of each parameter is less than the standard deviation. Not shown in the table are cathode voltage data, because the deviations for that quantity were less than one telemetry count. Table V data is interpreted as showing no change (within the measurement accuracy) of the OST rf output.

Beam Focusing

Measuring the current from the OST body to the PPS common (body current) gives an indication of beam dispersion. The body current measured at OST thermal stability for saturated output power at centerband frequency is shown in figure 8. The saturated output power condition is not a well defined or precisely controlled operating point (see General Procedure) and body current is sensitive to the operating point selected. Thus most of the deviation shown (about 5 percent) is accountable to minor variations in operating point conditions. Rf output is not sensitive to these variations. The body current comparison in table V indicates that within the measurement accuracy there is no perceptible change in beam dispersion and hence the beam focusing within the OST.

Cathode Life

Cathode aging is reflected as a decrease in beam current. The cathode of the 200-watt OST was expected to be one of the elements which would limit the life of the TWT. However, it was also expected that near 100 percent TEP time utilization was likely. Thus a cathode life of 20 to 25 thousand hours was required for 2 years operation. The beam current has decreased one telemetry count, 76.4 to 75.8 milliamperes, during the first 2 years in orbit. It had 10 950 hours operating time at 100 percent of rated power at the end of the 2-year period. This includes 1800 hours of pre-launch testing.

High Voltage Leakage

A high voltage leakage test is performed occasionally, about once per year, to determine if the high voltage insulators in the PPS and OST are becoming contaminated. The test is a comparison of the collector current sensor telemetry data with high voltage on and off. The test is performed with the cathode off. The current sensor resolution is 50 to 100 microamperes per count and the telemetry is noisy with variations of 2 to 3 counts. Thus, to increase the resolution the statistical frequency of each count was determined over a 5-minute period at each condition. It is expected that this method improves the resolution by a factor of 4, with some expected loss due to thermal drift.

During pre-launch tests and early on-orbit tests no change in leakage currents were observed. On January 15, 1978 small leakage current changes (25 to 50 microamperes) were observed on collectors 2, 7, and 8, but it is most likely that these were due to thermal drift. Comparison to subsequent test results will provide additional insight.

During pre-launch tests and early on-orbit tests the high voltages were monitored closely for anomalous operation that could be attributed to OST internal outgassing and subsequent high voltage breakdown. The anomalous operation would be indicated by shutdowns due to internal arcing. There was no evidence of arcing in these tests. OST internal pressure measurements are monitored continuously. There is a slight change in pressure from 5.1×10^{-8} to 7.7×10^{-8} torr when rf drive is applied but these pressures remained unchanged during the 2 years in space.

OUTPUT STAGE TUBE AND HEAT PIPE SYSTEM THERMAL PERFORMANCE

The purpose of this part of the investigation was to regularly monitor the thermal performance of the 200 watt OST and the VCHPS in important operating modes for several spacecraft orbit positions. Specifically, the objectives of this continuing effort are:

(1) To determine if critical component temperatures remain within prescribed limits.

(2) By comparison of current thermal characteristics with earlier ground and on-orbit data, to identify possible long-term performance changes.

(3) To identify thermal conditions that typify periods of communications use.

(4) To acquire current thermal characteristics data to aid in possible spacecraft problem diagnosis.

(5) To provide fundamental thermal performance data for application to future programs of a related nature.

Instrumentation

The locations of the thermal instrumentation routinely monitored to perform this investigation are identified in figures 9 and 10. The instruments (all thermistors except where noted) are identified in the figures and in the text by their computer-code descriptive symbols. In addition to the thermal instrumentation, the characterizations developed during this study required the use of quantities measured by other methods that are described elsewhere in this report. These other quantities include OST body current, OST input dc power, and OST output rf power and frequency.

Output stage tube. - As shown in figure 9, four thermistors are used to measure the temperatures on the OST. One of these, MDC1, is located on the cylindrical cover of the MDC section of the tube. This MDC cover is coated with a paint having a high thermal emittance and is cooled by direct radiation to space. Another thermistor, MDC2, is located on the MDC high-voltage feed-through flange just inboard of the MDC cover thermal choke (the bellows-like configuration in fig. 9). The remaining two sensors, BODY and CPLR, are attached to the heavy copper "isothermalizer" bar on the tube body at the output waveguide transformer position and at the output power diode sensor position on the output waveguide coupler, respectively.

Variable-conductance heat pipe system. - The VCHPS, shown schematically in figure 10, consists of the three variable-conductance heat pipes that transfer heat from an evaporator saddle located under the OST baseplate to an isolated radiator panel just adjacent and coplanar to the south spacecraft radiator panel. Six temperature sensors are located on the VCHPS, as indicated in figure 10. A thermistor is located on the adiabatic section of each heat pipe. These instruments, HP1T, HP2T, and HP3T, are attached to heat pipes designated 1 (shortest), 2, and 3 (longest), respectively. Thermistor HP4T is attached to heat pipe 1 a short distance (4 cm (1.57 in.)) further along the pipe from HP1T. Two additional temperature sensors, HP5T and HP6T, both platinum resistance thermometers, are positioned further along on heat pipe 1. Sensor HP5T is attached near (4 cm (1.57 in.)) the end of the inert-gas reservoir, and HP6T is attached directly to that reservoir.

A thermistor not shown, BPLT, located nearby on the baseplate of the power processor portion of the TEP is useful under some conditions as an additional indicator of VCHPS performance.

Test Procedures

The thermal testing program has consisted of three related efforts. These are OST thermal equilibrium tests, regular VCHPS checks at key operating periods, and continuous monitoring of several important OST and VCHPS temperatures.

OST thermal test conditions. - The OST thermal tests are all performed at the thermal equilibrium condition, since that condition provides a relatively repeatable comparison point. Further, since the test periods generally begin with the OST operating at other than the selected test condition, the time required for the OST to achieve thermal equilibrium is simultaneously determined during each test. A good knowledge of this thermal time characteristic is important for preeclipse operation planning to ensure that key OST temperatures remain in a safe range during eclipse periods.

Most of the thermal tests reported in this study were performed at the OST operating conditions expected to be most common. Specifically, these are saturated rf output power at center-band frequency (12.080 GHz), 100-watt rf output power (nominally, saturated minus 3 dB) at center-band frequency, and zero rf output power (the dc beam condition). Several tests at an intermediate power level, 180 watts at center band frequency, were also performed. In addition, saturated and 100-watt rf output power tests were also performed at the upper-band-edge (12.123 GHz) and lower-band-edge (12.038 GHz) frequencies, which are intended to represent worst-case (farthest from center-band frequency) operating conditions. With a few exceptions, the tests were performed while an unmodulated carrier signal was being transmitted.

Spacecraft orbital positions. - To allow data comparison, most of the OST thermal equilibrium tests were conducted at one of four selected spacecraft orbital positions which are separated by 90°. These orbital positions are shown schematically in figure 11. The first position, designated as 0°, is the spacecraft midnight position. Since prelaunch thermal vacuum tests at Lewis required approximately 2 hours for the OST to achieve thermal equilibrium after a condition change an on-orbit thermal test typically is begun about 1 hour before the spacecraft arrives at the desired orbital position and is continued about 1 hour beyond the desired position.

Each of the spacecraft orbital positions feature distinctly different solar illumination and solar array orientation conditions. These conditions directly affect the thermal environment of the spacecraft south panel radiator surface, the VCHPS radiator surface, and the OST MDC enclosure, which is also a radiator surface. The thermal conditions of these surfaces, in turn, directly affect the OST baseplate temperature and consequently the OST performance. Therefore, one of the objectives of this test series is to thermally characterize the OST and VCHPS relative to operating conditions for each of the selected orbital positions. This information may be required

for the interpretation of any effects that are regarded as unusual during later operation during user and technology experiments.

Sun angle effects. - Because the Sun incidence angle relative to the spacecraft orbit plane progressively changes throughout the year, the spacecraft experiences day-by-day changes in thermal environment independent of the orbital position and the OST operating conditions. Therefore, in addition to the requirement of determining the thermal characteristics of the OST and VCHPS for the various operating conditions and spacecraft orbital positions, the effects of the variation of the solar flux incidence angle must also be determined for complete characterization.

VCHPS condition monitoring. - In addition to the VCHPS temperature data taken during the OST thermal equilibrium test periods, the several temperatures that define the performance of this thermal control system are examined frequently. This examination is particularly necessary when the OST experiences changes in operating conditions that rapidly change VCHPS temperatures. Such situations, for example, occur at OST turnon periods, particularly after a relatively long period when the OST has not been operated. The objective of this monitoring is to regularly evaluate the starting and operating conditions of the VCHPS and to document the anticipated long-term degradation of the optical properties of the radiator.

Several VCHPS and OST temperatures are also monitored continuously on strip-chart recorders and are regularly examined. This monitoring is done to ensure that unanticipated temperature excursions that might occur during nonspecific thermal test periods can be quickly detected and evaluated.

Output-Stage-Tube Thermal Test Results

As has been indicated, the OST tests were all performed at the thermal equilibrium condition. That condition is defined as that time when all monitored OST temperatures remain stable within 1° C for at least 5 minutes. For most of the tests performed, the monitored VCHPS temperatures met this criterion as well. As noted in reference 2, approximately 2 hours was required for the OST to achieve thermal equilibrium following an operating condition change in the early life of the spacecraft. This characteristic has remained essentially unchanged over the 2-year period, as evidenced by the data in figure 12. This figure shows the time-temperature characteristics of the OST body (BODY), the two MDC instrument locations (MDC1 and MDC2), the output waveguide coupler (CPLR), and the adiabatic section of heat pipe 1 (HP1T) during a startup transient and continuing until essential thermal equilibrium is attained. The test conditions were saturated rf output power at center band frequency. Just prior to the start of the test, the OST had been in the "standby" mode, with only the cathode heater at 50 per-

cent power (about 2 W) for some time. As a result, the OST and VCHPS temperatures were all at a relatively depressed level. The perturbations observed in several of the temperatures of figure 12 between 7 and 22 minutes were caused by a brief (about 5 min) uplink power reduction for ground station equipment adjustment. In general, the OST thermal data presented in this report are the first data points taken after the requirement of thermal equilibrium has been met.

Because of the day-by-day variation of the Sun incidence angle with the spacecraft orbital plane, it is not possible to rigorously evaluate by comparison the results of thermal tests run at identical OST operating conditions even a few days apart. In order to establish a basis for data comparison as a function of time, test results will only be compared for periods with like Sun incidence angles. These periods are shown graphically in figure 13. The time intervals during the negative Sun angle periods are denoted as "A" periods, while the positive Sun angle periods are denoted as "B" periods. Each period designation is suffixed by the last two digits of the calendar year in which the period ended. Only test data taken in similar Sun angle periods (i.e., A76, A77, and A78) will be compared.

As time progressed, a number of factors contributed to a reduction in the frequency of thermal stability testing relative to the early life of the spacecraft (ref. 2). An intentional reduction in testing, partly to afford other experimenters adequate spacecraft access time for their studies was one factor. In addition, a reduction in the output power of the spacecraft telemetry transmitters became significant in the early months of 1977. Starting at that time, support in obtaining reliable telemetry data was required from other United States spacecraft-monitoring facilities, causing scheduling complications and resulting in even fewer regularly-scheduled tests. This reduction in thermal testing frequency as time progressed is reflected in table VI which summarizes the number of thermal stability tests performed during all the positive and negative (B and A, respectively) Sun angle periods.

In order to present the experimentally-determined TEP thermal characteristics in a comprehensive manner, the temperature data in this report will be plotted as a function of spacecraft orbital position, and parametrically with testing periods. Not every specific test data point at every condition is presented in the plots, but those points which are presented are typical of all the data at that particular test condition. The data represented in this report is that taken over the entire first 2 years of TEP on-orbit operation. Therefore, some of this data is also included in the report describing the thermal, rf, and electrical performance of the TEP for the first 90 days of on-orbit operation, reference 2.

Saturated rf output power, center band frequency conditions. - Since it provides the maximum rf output power and overall efficiency, the saturated rf output power, center band frequency TEP operating condition has been a principal test point since the start of on-orbit operation as indicated in table VI. A summary of the TEP temperature data taken at saturated rf output power at center band frequency is presented in figures 14(a) to (e).

Equilibrium temperature profiles for the MDC cover temperature, MDC1, are shown in figure 14(a). The MDC cover temperature variation for essentially constant operating conditions as a function of spacecraft orbital position is attributable to the differences in solar illumination on the cover. Figure 14(a) shows that the MDC cover receives very little direct solar illumination at the 0^{o} orbital position but that maximum illumination is experienced at the 180^{o} position. Consequently, the maximum and minimum MDC cover temperatures occur at the 180^{o} and 0^{o} orbital positions, respectively.

Figure 14(b) presents the equilibrium temperature profiles for the adiabatic section of heat pipe 1, HP1T. When heat pipe 1 is active (HP1T $\gtrsim 25^{o}$ C, approx.) HP1T approximates the OST baseplate temperature. The HP1T temperature profiles shown in figure 14(b) are fairly level except for a slight depression at spacecraft orbital positions other than 0^{o}. At 0^{o} the inboard heat pipe radiator surface receives a greater amount of reflected solar illumination than at other orbital positions. The HP1T temperature profiles for the positive Sun angle cases are generally lower than their negative Sun angle case counterparts because of the lack of direct solar illumination of the south surfaces of the spacecraft and the VCHPS radiator. The lowest temperature on the positive Sun angle profiles is at the 180^{o} orbit position, where the VCHPS radiator is completely in the shadow of the spacecraft body.

Equilibrium profiles for the OST body temperature, BODY, and the output waveguide coupler temperature, CPLR, are shown in figures 14(c) and (d), respectively. Since these instrument locations are conductively closely-coupled, the shape of the temperature profiles are similar. The CPLR temperature is generally higher, largely because of its more remote location from the VCHPS saddle on which the OST is mounted. The influence of the low heat pipe temperature, HP1T, at the 180^{o} spacecraft orbit position is apparent on the positive Sun angle profiles of figures 14(c) and (d).

The location of the instrument (MDC2) on the MDC high-voltage feed-through flange is also conductively close-coupled to the OST body; therefore the temperature profile for MDC2 (fig. 14(e)) bears a strong resemblence to that of the BODY and CPLR temperatures. The effect of its conductive coupling to the MDC cover, however, apparently influences the MDC2 temperature profile as well, causing a modest increase

in temperature at the 180° spacecraft orbit position relative to the other positions for the negative Sun angle periods. At the 180° orbit position, of course, the MDC cover experiences maximum solar illumination. At positive Sun angles, the MDC cover experiences shadowing by the apogee motor and support structure at the 180° orbit position, causing the depressed MDC2 temperature at that orbit position indicated in figure 14(e). Again, the influence of the heat pipe temperature characteristic is apparent in figure 14(e), particularly for the negative Sun angle case.

Figures 14(c) to (e) all indicate a relatively small, but apparently consistent, increase in temperature for the BODY, CPLR, and MDC2 instrument locations for essentially identical test conditions at successive test periods for both the negative and positive Sun angle cases. Since this apparent trend is not accompanied by a measurable companion increase in either OST body current or heat pipe 1 adiabatic section temperature (HP1T, taken to be approximately equal to OST baseplate temperature), a suggestion which presents itself is that one or more of the several thermal interfaces within the OST structure have become compromised by aging and/or the 2 years of temperature cycling which occurs during normal day-to-day TEP operations. These interfaces are described in detail in reference 2. The result of interface degradation could be an increase in measured component temperature without a noticeable change in OST baseplate temperature. It must be noted, however, that because of the very small data sample available, the statistical significance of this apparent trend is questionable. Certainly, further testing would be required to permit a confident assessment of these trends.

100 watt rf output power, center band frequency conditions. - The second-most-frequently repeated thermal stability test condition, as indicated in table VI, has been the 100 watt rf output power, center band frequency operating condition. A summary of the TEP temperature data taken at this condition during the first 2 years of on-orbit operation is presented in figures 15(a) to (e). Except for obvious differences in temperature levels, the characteristics of this data are similar to those for the saturated rf output power, center band frequency conditions discussed earlier.

Figure 15(a) displays the equilibrium profiles for the MDC cover temperature, MDC1, as a function of spacecraft orbit position for both the positive and negative Sun angle cases. As with the MDC temperature characteristics shown in figure 14(a), the influence on the MDC1 temperature of solar illumination as a function of orbit position is significant. Here also, the MDC1 temperature is high at the 180° orbit position and low at the 0° position, where direct solar illumination is maximum and minimum, respectively. The general level of the temperatures in figure 15(a) is higher than that of figure 14(a) because of more beam power available in the collector at conditions other than saturated rf output power, center band frequency. This characteristic is demonstrated for several operating conditions in reference 2.

The equilibrium temperature profiles for the adiabatic section of heat pipe 1, HP1T, are presented in figure 15(b). While the general characteristics of these profiles are similar to those of the saturated rf output power, center band frequency condition shown in figure 14(b), the temperature levels of figure 15(b) are lower. This is because of the lower rf output power level and consequently lower body current level at the latter condition.

It has been indicated that the temperature-measurement locations represented by the OST body, BODY, the rf output waveguide coupler, CPLR, and the MDC high-voltage feed-through flange, MDC2, are conductively closed-coupled. Further, while the MDC2 location is primarily influenced by the thermal condition of the OST body, it also is moderately affected by solar illumination of the MDC cover. The equilibrium temperature profiles for BODY, CPLR, and MDC2 are presented in figures 15(c) to (e), respectively. Because of the lower heat input rate to the body of the OST at the 100 watt rf output power relative to the saturated rf output power level, the temperature profiles of figures 15(c) to (e) are lower than those of figures 14(c) to (e), respectively. Each of the temperature profiles is affected at orbit positions other than 0^{o} by the depressed temperature characteristic of HP1T at those positions noted earlier.

The data sample for the thermal equilibrium tests at the 100 watts rf output power at center band frequency operating condition is even smaller than that for the saturated rf output power condition at the same frequency. With this qualification in mind, it is noted that the apparent increase in temperature for the BODY, CPLR, and MDC2 instrument locations for essentially identical test conditions at successive test periods for both positive and negative Sun angle cases is also suggested by this data.

Other Test Conditions

In addition to the TEP thermal stability tests conducted at the saturated and 100-watt rf output power levels at the center band frequency conditions, a number of tests were also performed at several other conditions. Table VI indicates the other thermal stability tests were conducted at saturated and 100-watt rf output power levels at upper and lower band edge frequencies and the dc beam (zero rf output power) conditions. In addition, tests at 180 watts rf output power at center band frequency were also conducted during the last two sun angle periods indicated in table VI. With the exception of the 180 watt rf output power condition, most of the data for these other tests was acquired during the first 90 days of on-orbit TEP

operation and was discussed in reference 2. The few additional tests performed since reference 2 at other than the saturated and 100 watt rf output power conditions at center band frequency do not merit separate graphical presentation. The data from these tests, however, taken along with earlier data, does provide a useful index of typical temperature ranges which can be expected for the body, CPLR, MDC1, MDC2, and HP1T temperature locations for the negative and positive sun angle cases for the operating conditions tested (table VII). The wide temperature range indicated for MDC1 reflects the significant influence of spacecraft orbit position on this parameter, particularly for the negative sun angle case. Excluding MDC1, all the other parameters display a generally lower-level temperature for the positive sun angle case. This is clearly due to the lack of direct solar illumination on the spacecraft south-facing radiator panel and the reduced direct illumination of the VCHPS radiator for the positive sun angle case. It was noted that HP1T is taken to be representative of the OST body temperature when HP1T is active. Table VII shows that heat pipe 1 is apparently not active at the low OST body heat-rejection-rate level of the dc beam tests for the positive sun angle case. The HP1T temperatures for these tests are, therefore, not indicative of the OST baseplate temperature.

Significant excursions of parameter values away from those ranges shown in table VII may be viewed as possible indications of OST, PPS, or VCHPS performance changes.

VARIABLE-CONDUCTANCE HEAT PIPE SYSTEM THERMAL PERFORMANCE

As has been described, the VCHPS transfers heat from an evaporator saddle located beneath the OST baseplate to an isolated radiator panel adjacent and coplanar to the south-facing spacecraft radiator panel. The system is shown schematically in figure 10. The three heat pipes, designated 1 (shortest), 2, and 3 (longest) are dual-artery, stainless-steel pipes. Methanol is the medium fluid and a mixture of nitrogen (90 percent) and helium (10 percent) is the inert regulating gas. The system is designed so that as heat input to the evaporator saddle is increased from very low levels, heat pipe 1 becomes active first, followed by pipes 2 and 3 in that order. As the heat input is increased, the active length of the pipes and, consequently, the active area of the radiator to which the pipes are attached increase. With this system, the heat pipes are considered to become active, or turn on, when the temperatures indicated at the locations of HP1T, HP2T, and HP3T reach a level of about 25° to 30° C. The active length of heat pipe 1 is intended to be indicated by the three other temperature sensors located further along its length - HP4T, HP5T, and HP6T.

VCHPS Startup and Shutdown Characteristics

Figure 16 presents time profiles of the VCHPS temperatures HP1T, HP2T, HP3T, HP4T, HP5T, and HP6T, as well as the OST body temperature, BODY for approximately 2 hours following the TEP turn-on described in the section "Output-Stage-Tube Thermal Test Results." Since the TEP had been in "standby" mode prior to the turnon, the VCHPS radiator had been cooling from its earlier level. This resulted in the falling temperatures for the VCHPS sensors until about 0922 EDT. At that time, the gas-vapor front advancing from the evaporator saddle reached the HP1T sensor location and resulted in the abrupt temperature increase to about 25° C. About 4 minutes later, temperatures HP2T and HP3T experienced similar but less rapid increases as heat pipes 2 and 3 also became "active." Then, as the gas-vapor front in heat pipe 1 advanced to the HP4T sensor location at about 0928 EDT, that temperature also increased abruptly. At the end of about 2 hours, OST thermal stability was achieved, as evidenced by the OST body temperature curve shown in figure 16. At that point, the values of HP1T, HP2T, and HP3T stabilized at levels of about 31°, 33°, and 34° C, respectively. The temperature HP4T, located on heat pipe 1, stabilized at the level of HP1T. Sensors HP5T and HP6T, located on the inactive length of heat pipe 1, were not affected by the OST body heat rejection.

The behavior of the VCHPS during the OST turn-on sequence illustrated in figure 16 is recognized as being essentially identical to that observed during early on-orbit experience (ref. 2). With the exception of a "special-case" type of TEP thermal anomaly, the VCHPS has to at the time of this report function thermally as designed, turning on and off as required to maintain the temperature of the components of the TEP (including the OST) within the limits prescribed in reference 4. The anomalous performances of the VCHPS will be treated in the following section of this report.

TEP THERMAL ANOMALIES

As indicated in the previous section of this report, the TEP has experienced some thermal anomalies, or significant deviations from normal thermal behavior while in orbit. These anomalies occurred on four occasions during 1977 - on days 75 (March 16), 82 (March 23), 101 (April 11), and 253 (September 10). During these occurrences, the OST body temperature, BODY, and nearby temperatures CPLR and MDC2 (refer to fig. 9) experienced sudden, unexpected, and rapid increases

from their normal levels for the operating conditions at the time. The temperatures continued to increase toward structure-threatening levels until terminated by a change in TEP operating conditions. Figure 17 shows the rapid OST body temperature increase during the first anomaly observed, and which was essentially typical of all the anomalous behavior occurrences. This initial rise, at the rate of about 1.5^{o} C/min began at the normal temperature of 56^{o} C for the operating conditions at the time. Over a period of about 38 minutes, the temperature rose to 75^{o} C, at which point the OST rf output power level was reduced to zero, and the affected temperatures were reduced to a safe level. Each of the four anomalies was terminated with no apparent TEP damage, and normal TEP operation was resumed shortly (within 1 hr) after each event. No additional TEP thermal anomalies have occurred since the last date noted.

Concern over the TEP thermal anomalies prompted an urgent, extensive investigation into their cause, impact, and methods of prevention. Extensive ground component testing, data analysis, and on-orbit tests have indicated that temporary malfunctions of the VCHPS which provides the principal OST thermal control caused the anomalies. This investigation is reported in reference 5. The following paragraphs very briefly outline some of the salient points of that study.

Figure 10 shows the position of the OST relative to the VCHPS and other spacecraft features. As described earlier, the tube body is mounted on the VCHPS evaporator saddle which in turn is mounted on the spacecraft south-facing panel next to the PPS. The VCHPS radiator is coplanar to the south panel and essentially coplanar to the earth equatorial plane. Experiments have demonstrated that depriming, or interrupting operation of the heat pipe internal dual fluid-carrying arteries abruptly decreases the heat-carrying capacity of VCHPS to about 106 watts, while the OST body rejects about 155 watts while operating at the saturated rf output power, center band frequency condition. The difference between these two heat-rejection rates corresponds well to the observed OST body temperature rate of increase during an anomaly at the described operating condition.

The shaded portion of the CTS spacecraft orbit shown in figure 11 indicates the angular arc in which all the TEP thermal anomalies have occurred. Since all the anomalies have occurred during the spring and fall spacecraft earth-eclipse seasons, the sun angles with the spacecraft orbital plane have been small. This resulted in the VCHPS radiator being at least partially shadowed by the spacecraft body prior to and during the anomalies, with minimum solar heat input to the radiator. Several heat-pipe-artery-depriming mechanisms dependent on low temperatures have been postulated, but the exact cause or combination of causes for the depriming has yet to be identified.

The investigation reported in reference 5 identified the most likely cause of the dangerous and unexpected TEP thermal anomalies, as well as the most likely combination of circumstances for the anomalies to occur. Briefly, the anomalies are most likely to occur from 14:00 to 19:30 GMT, when the sun angle with the spacecraft orbit plane is between -4^{o} and 10^{o}, and when the OST rf output power level is that which will give rise to an OST body heat rejection rate greater than 106 watts. This critical heat-rejection rate, to repeat here, is the maximum rate which the VCHPS can sustain in a deprimed-artery state. Ground component testing has determined this critical OST body heat-rejection rate is exceeded when the rf output power is greater than 140 watts at center band frequency, 127 watts at upper band edge frequency, or 157 watts at lower band edge frequency.

Based on these considerations, and others, safe TEP operating procedures have been established and are rigidly observed during anomaly-susceptible periods.

COMMUNICATIONS CHARACTERISTICS

The long-term stability of communications characteristics is evaluated by the regular performance of two tests, the frequency response and power transfer characteristics tests, and an occasional performance of the single channel video test. The latter test was performed once in 1976 and once in 1977 and the measured values of signal-to-noise ratio, differential gain and differential phase were compared. These measurements were made at three points in the transmit/receive band (uplink frequencies 14.226, 14.247, and 14.268 GHz) and six output power levels ranging from SAT +2 dB to SAT -3 dB in 1.0 dB steps. The differences were too small to conclude that a change in characteristics had occurred.

Although the frequency response and power transfer characteristics are measured regularly only samples of the results are shown in figures 18 and 19. The solid line is the result of a thermal vacuum test of the fully integrated spacecraft before launch. The difference of the frequency response (in fig. 18) between thermal vacuum and on orbit data represents the change in measurement system response between ground and on orbit systems. The spread in the on orbit data is due to measurement system variations. It should not be interpreted as a change in characteristics.

The spread in the power transfer characteristics (fig. 19) is due to the uplink noise power contribution to the characteristics at low drive levels when attenuator no. 2 is 0 dB. Note that when attenuator no. 2 is at 5 dB, there is 5 dB more carrier power increasing the carrier to noise ratio by 5 dB and the on orbit characteristics approach that of the OST in bench tests before launch.

SUMMARY OF RESULTS

The assessment of TEP operation after 2 years in orbit is that it is still operating satisfactorily as indicated by electrical and communications tests. The TEP has accumulated 10 950 hours of actual operating time in orbit and 1800 hours in ground tests. Two anomalous operating difficulties have been experienced, the inconsistency of on-board rf power measurements (FRWD) over 200 watts and occasional abnormal excursion of the body temperature. Otherwise the TEP has operated extremely well. Electrical tests have shown no measurable change in PPS efficiency, OST efficiency, rf output power, beam focusing or high voltage leakage. The beam current has decreased one telemetry count (0.8 percent) which indicates that the cathode will meet or surpass the cathode life expectancy.

Communications tests have shown that the frequency response and power transfer characteristics have not changed. A single channel video test affirmed that picture quality was the same in 1977 as it was in 1976.

THERMAL PERFORMANCE

The following observations were made:

1. A specific combination of TEP operating conditions and spacecraft orbit positions has been shown to have led to four separate temporary thermal control system malfunctions from which recoveries were made without component damage. Excluding these incidents, which have been shown to be avoidable, the TEP thermal performance continues to be satisfactory throughout the first 2 years of on-orbit operation. Specifically, measured key TEP component temperatures remained well within the limits established for worst-case flight predictions at all operating conditions examined. Based on a relatively small data sample, however, there appears to be a small increase in OST body, waveguide coupler, and MDC high-voltage feedthrough flange temperature for given operating conditions relative to early on-orbit experience. These apparent increases are from 5^{o} to 10^{o} C for the saturated rf output power, center band frequency operating condition. If this observation is valid, the trend may indicate a long-term compromise in OST thermal interface quality, particularly since apparently the temperature increase is not accompanied by an increase in OST body current or baseplate temperature.

(The anomalous TEP thermal behavior noted in the previous paragraph was the subject of a separate investigation and has been shown to be caused by temporary abrupt reductions in the heat-carrying capacity of the VCHPS. The most likely circumstances for such an anomaly to occur are for the

sun angle relative to the spacecraft orbit plane to be between -4^{o} and 10^{o} during the time period 14:00 to 19:30 GMT, while the OST body heat-rejection rate exceeds 106 watts. This critical heat-rejection rate is exceeded if the OST rf output power exceeds 140 watts at center band frequency, 127 watts at upper band edge frequency, or 157 watts at lower band edge frequency. Avoidance of this combination of conditions has been shown to preclude anomalous TEP thermal performance.)

2. Typical OST and VCHPS temperatures or ranges of temperatures have been established for the various operating conditions examined in this study. These temperature ranges represent an expansion and update of similar ranges developed for the early (first 90 operating days) TEP on-orbit operating experience. In most cases, the more recent data reflects a small temperature increase for the parameters, as described in item 1 above. Significant departures from these typical ranges may indicate OST and/or VCHPS performance changes.

3. As in early on-orbit TEP experience, approximately 2 hours was required for the OST to achieve essential thermal equilibrium after an operating condition change. The TEP rf performance was normal throughout an OST thermal transient period.

4. The VCHPS continued to function thermally as designed throughout the first 2 years of on-orbit operation, with the exception of the four anomalous occurrences noted in item 1 above. The VCHPS turned on and off as required to maintain the temperatures of the TEP components within safe prescribed limits.

REFERENCES

1. Alexovich, R. E.: The 200 Watt SHF Transmitter Experiment Package. NASA TM X-68106, 1972.
2. Early Performance of the 12-GHz, 200-Watt Transmitter Experiment Package in the Communications Technology Satellite. NASA TM X-3555, 1977.
3. Kosmahl, Henry G.: A Novel, Axisymmetric, Electrostatic Collector for Linear Beam Microwave Tubes. NASA TN D-6093, 1971.
4. Chomos, Gerald J.; and Curren, Arthur N.: Description and Expected Performance of Flight-Nodel, 12-Gigahertz, Output Stage Tube for the Communications Technology Satellite. NASA TM X-3441, 1976.
5. Alexovich, R. E.; and Curren, Arthur N.: Thermal Anomalies of the Transmitter Experiment Package on the Communications Technology Satellite. NASA TP-1410, 1979.

TABLE I - POWER-PROCESSING-SYSTEM PERFORMANCE CHARACTERISTICS

Converts 28-V and 76-V dc power to -
Nine high-voltage collector supplies (cathode voltage, -11.3 kV; current, 72 mA; regulation, ±1 percent; ripple, 0.01 percent)
Cathode heater supply (voltage, 4 2 V, current, 1.5 A; floating at -11 3 kV)
Anode supply (voltage, 350 V ± 200 V, current, 100 mA)
Ion pump supply (voltage, 4 kV, current, 50 μA)
Protects system against -
Excessive current in output stage tube
Excessive pressure in output stage tube
Excessive arcing
High or low voltage on input lines (tolerates 95 and 45 V)
Power conversion efficiency, 86.56 percent to 88 51 percent

TABLE II - TRANSMITTER-EXPERIMENT-PACKAGE TELEMETRY DATA SUMMARY

Cathode heater voltage, V dc	0 - 10
Cathode voltage, kV	0 - -15
Beam current, mA	0 - 100
Output-stage-tube body current, mA	0 - 15
Anode voltage, V dc	0 - 600
Collector voltages (3), kV	0 - -10
Collector currents (10), mA	0 - 40
Output-stage-tube and power-processing-system temperatures, ^{o}C (^{o}F)	-55 - 225 (-65 - 435)
Radiofrequency power (2), W	0 - 250
Output-stage-tube internal pressure, N/m^2 (torr)	1.33×10^{-4} - 1.33×10^{-6} (10^{-6} - 10^{-8})
Bus currents, A	0 - 10
Heat-pipe temperatures (6), ^{o}C (^{o}F)	-73 - 93 (-100 - 200)

TABLE III. - OUTPUT STAGE TUBE

PERFORMANCE SPECIFICATIONS

Nominal radiofrequency output power, W	200
Efficiency goal, percent	50
Center-band frequency, GHz	12.0805
Bandwidth (3 dB), MHz:	
Minimum	85
Maximum	250
Saturated gain, dB	30
Small signal gain variation (peak to peak), dB	5
Second-order phase deviation, deg/MHz^2	0.2
Noise figure, dB	40

TABLE IV. - SUPER HIGH-FREQUENCY GROUND-STATION CHARACTERISTICS

Location:	
Area	Lewis Research Center, Cleveland, Ohio
Latitude	$41^{o}24'45''$ N
Longitude	$81^{o}51'55''$ W
Elevation, m (ft)	231 (758)
Antenna:	
Type	Parabolic reflector with Cassegrain feed
Diameter, m (ft)	5 (16)
Polarization	Linear orthogonal (transmit/receive)
Mount	Elevation over azimuth
Receiving frequency, GHz	11.7 to 12.123 (11.7 Beacon) 14.0 to 14.3
Transmitting frequency	14.150 GHz ± 150 MHz
Gain to temperature ratio, dB	27.6
Gain (receive), dB	53.0
Gain (transmit), dB	54.4
Receiving system noise temperature, K	343
Effective isotropic radiated power (EIRP), dBW	85
Beam width (3 dB), deg:	
Receive	0.37
Transmit	0.32
Tracking accuracy (step track), deg	±0.05
Transmitter:	
Frequency, GHz	14
Modulation	FM
Maximum power output, kW	1.25
Radiofrequency bandwidth, MHz	85
Modulators (two each):	
Frequency, GHz	14
Modulation	FM
Power output, dBm	22.6
Subcarriers (audio), MHz	7.5, 5.14, 5.41, 5.79
Preemphasis:	
Video	CCIR
Audio, μsec	75
Deviations (peak to peak):	
Video, MHz	10 - 30
Carrier by subcarrier, MHz	2 4
Subcarrier by audio, kHz	120 - 200
Demodulators (two each)[a]:	
Frequency, GHz	12
Modulation	FM

[a]Compatible with modulators, except for frequency.

TABLE V. - COMPARISON OF COMPUTED MEAN OF OST DATA FROM THERMAL STABILITY TESTS

	First year			Second year		
	No. of points	Mean	Standard deviation	No. of points	Mean	Standard deviation
OST output power, W	29	218.13	6.25	22	216.08	5.16
OST input power, W	29	466.2	10.20	19	468.3	9.03
OST efficiency,[1] percent	36	32.76	.82	8	33.29	1.29
PPS efficiency, percent	29	85.28	.84	19	85.81	.93
OST body current, mA	29	6.312	.434	19	6.504	.279

[1]At 100 watts OST output power.

TABLE VI. - TIME DISTRIBUTION OF TEP THERMAL STABILITY TESTS PERFORMED DURING FIRST 2 YEARS OF CTS OPERATION

TEP operating conditions	Number of tests during each time period																			
	A76				B76				A77				B77				A78			
	Orbit position				Orbit position				Orbit position				Orbit position				Orbit position			
	0^o	90^o	180^o	270^o	0^o	90^o	180^o	270^o	0^o	90^o	180^o	270^o	0^o	90^o	180^o	270^o	0^o	90^o	180^o	270^o
Saturated rf output center band frequency	1	2	5	2	3	3	3	4	2	1	1	2	2	3	4	3	0	3	2	2
Sat, upper band edge	1	0	0	0	3	2	3	3	1	1	1	2	0	0	0	0	0	0	0	0
Sat, lower band edge	0	0	1	1	3	2	2	2	1	1	0	1	0	0	0	0	0	0	0	0
100 W, center band	1	1	1	1	2	2	2	3	1	2	2	2	0	1	0	0	0	0	0	0
100 W, UBE	0	0	0	0	2	2	2	2	1	1	0	0	0	0	0	0	0	0	0	0
100 W, LBE	0	0	0	0	2	2	1	2	1	0	1	0	0	0	0	0	0	0	0	0
DC beam (zero rf)	1	1	1	1	2	2	2	2	0	0	1	0	0	0	0	0	0	0	0	0
180 W, CB	0	0	0	0	0	0	0	0	0	0	0	0	0	1	0	1	4	0	1	2
Total	21				65				26				15				14			

Notes: A76· Feb. 8, 1976 - Mar. 21, 1976
B76· Mar. 21, 1976 - Sep. 21, 1976
A77· Sep. 21, 1976 - Mar. 21, 1977
B77 Mar. 21, 1977 - Sep. 21, 1977
A78 Sep. 21, 1977 - Feb. 8, 1978

TABLE VII. - EQUILIBRIUM THERMAL OUTPUT-STAGE-TUBE AND VARIABLE-CONDUCTANCE HEAT PIPE SYSTEM CHARACTERISTICS

Radio-[3] frequency output	Operating[1] frequency	Transmitter-experiment package input power (typ), W	Body current (typ.), mA	Temperature range (low to high),[2] °C									
				BODY		CPLR		MDC1		MDC2		HP1T	
				Neg sun angle	Pos sun angle	Neg sun angle	Pos. sun angle	Neg sun angle	Pos. sun angle	Neg. sun angle	Pos. sun angle	Neg. sun angle	Pos. sun angle
Saturation (typ. 217 W)	Center band	468	6.4	56-64	50-62	80-89	73-86	139-180	134-160	70-84	65-74	31-43	27-41
Saturation (typ. 158 W)	Upper band edge	403	5.3	55-60	50-58	75-80	69-75	142-189	142-160	66-76	61-69	33-43	29-39
Saturation (typ. 188 W)	Lower band edge	475	5.8	53-63	50-59	78-89	76-85	147-185	146-162	73-76	65-71	33-43	27-41
~180 W	Center band	413	4.5	53-62	51-53	75-83	73	127-185	147-160	70-73	63-68	35-43	33-35
~100 W (Nom. saturation minus 3 dB)	Center band	309	2.5	44-50	39-47	57-64	51-58	156-201	159-168	55-69	51-58	29-39	25-37
	Upper band edge	308	3.1	47-52	41-49	61-66	52-61	155-169	156-164	62-63	53-59	31-41	25-37
	Lower band edge	318	2.4	43-50	39-47	59-64	53-59	159-196	159-172	60-64	52-59	27-39	25-37
~0 W (direct current beam)	Not applicable	171	1.7	35-40	31-36	38-41	33-35	163-201	160-168	45-55	39-43	27-33	-15-24

[1]Center band, 12.080 GHz, upper band edge, 12.123 GHz, lower band edge, 12.038 GHz.
[2]Refer to text for instrument locations.
[3]Refer to rf power measurements section of report.

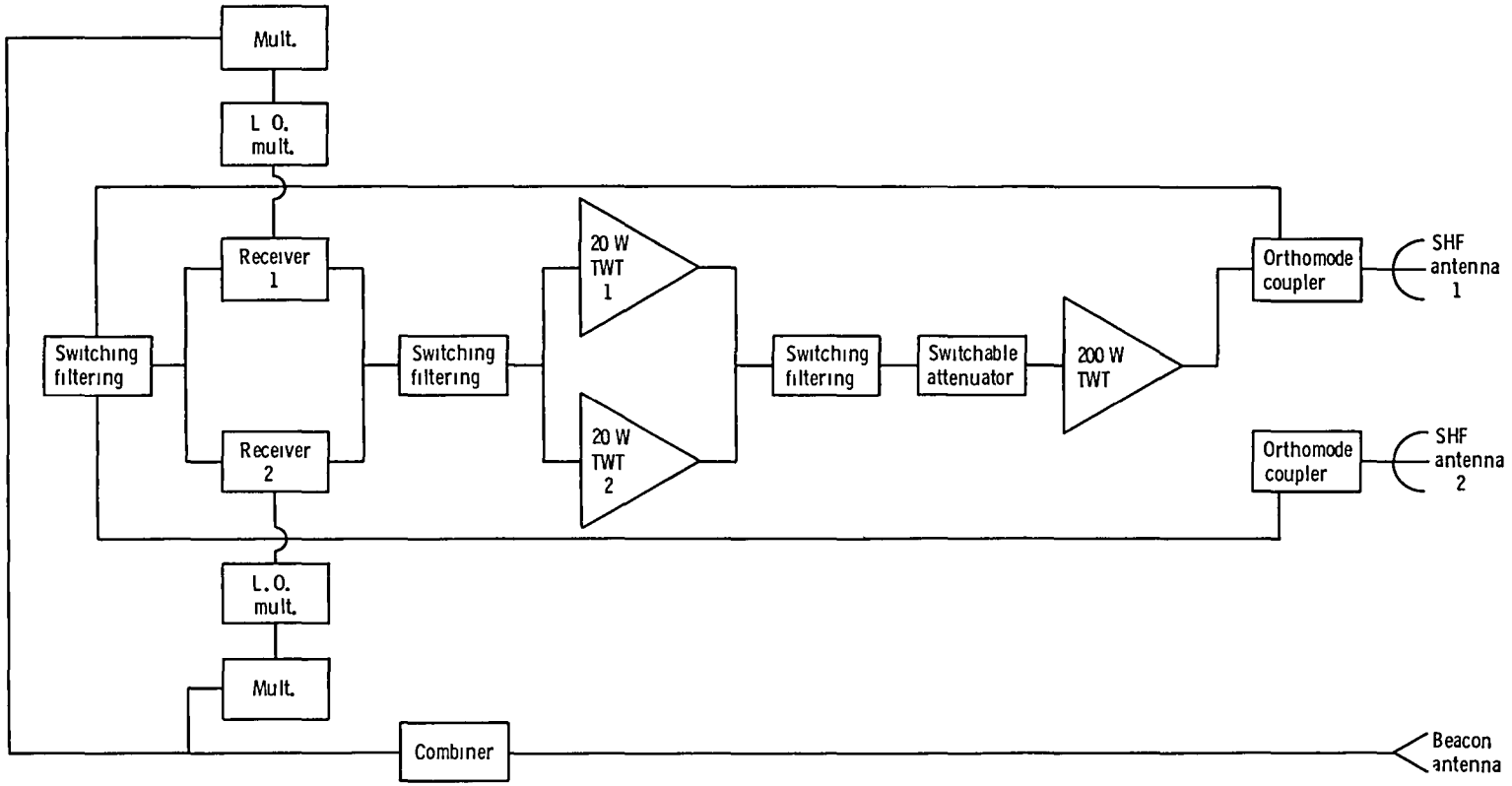

Figure 1. - Block diagram of super high frequency transponder.

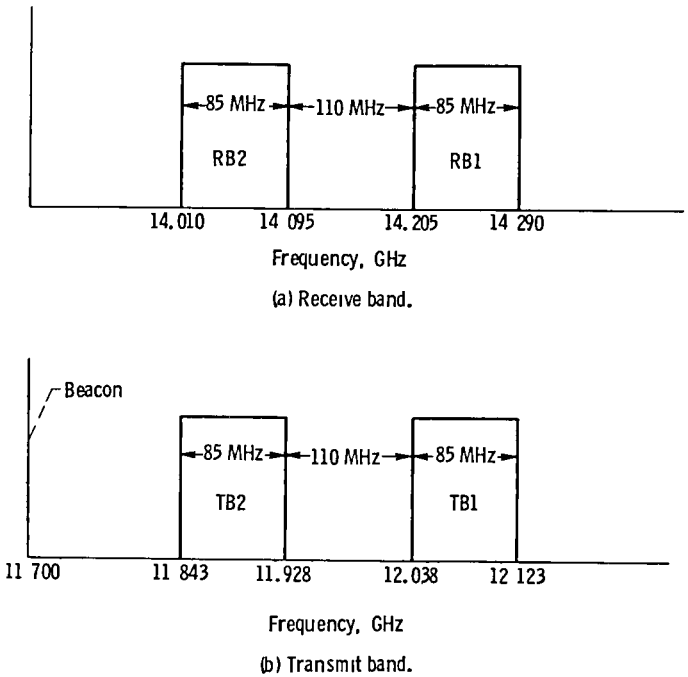

Figure 2 - Transponder frequency plan.

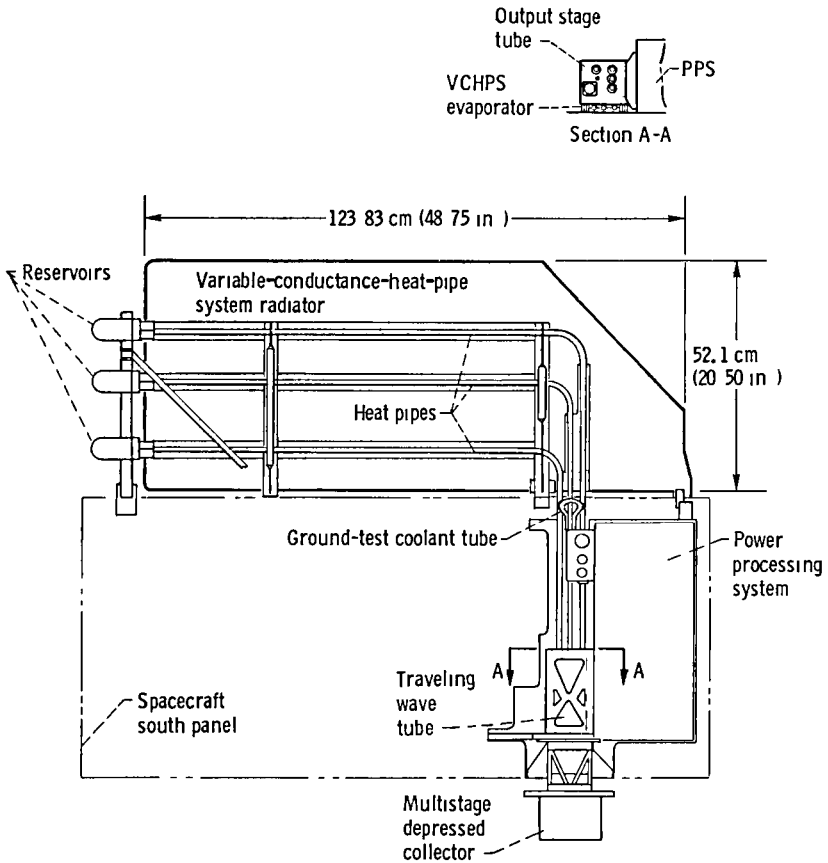

Figure 3 - Transmitter experiment package and variable-conductance heat pipe subsystem

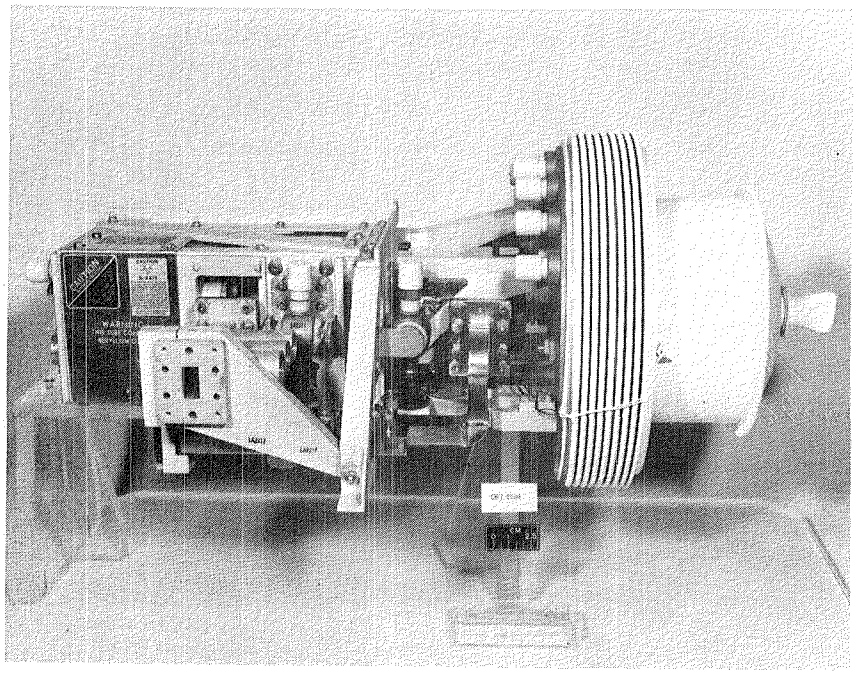

Figure 4. - Output stage tube.

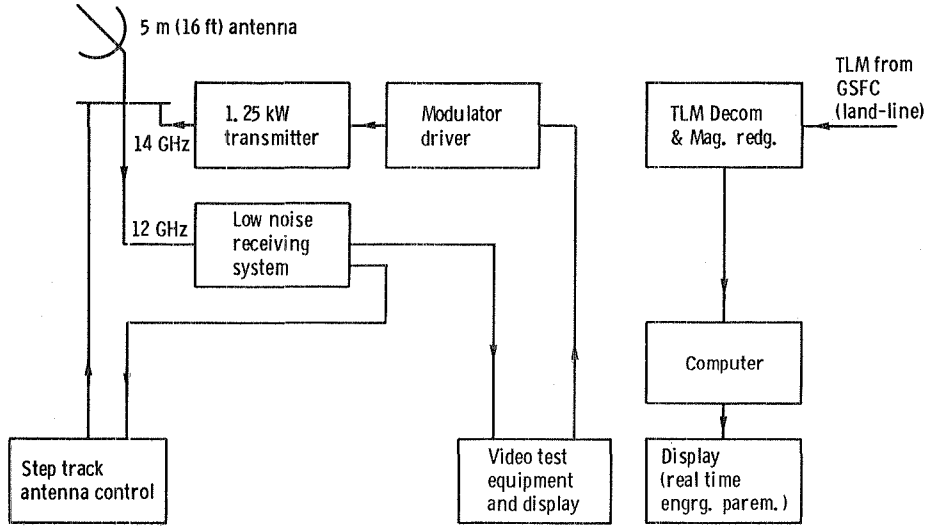

Figure 5. - NASA ground station, functional block diagram.

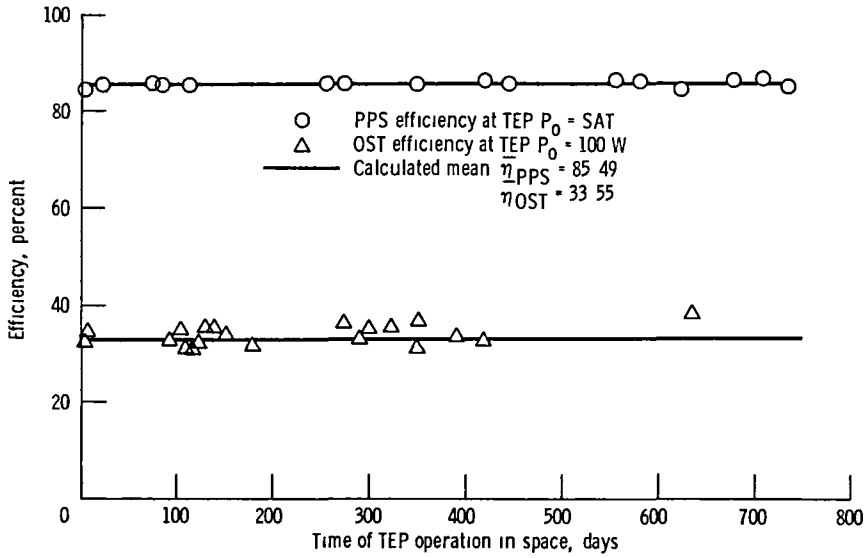

Figure 6 - PPS and OST efficiency

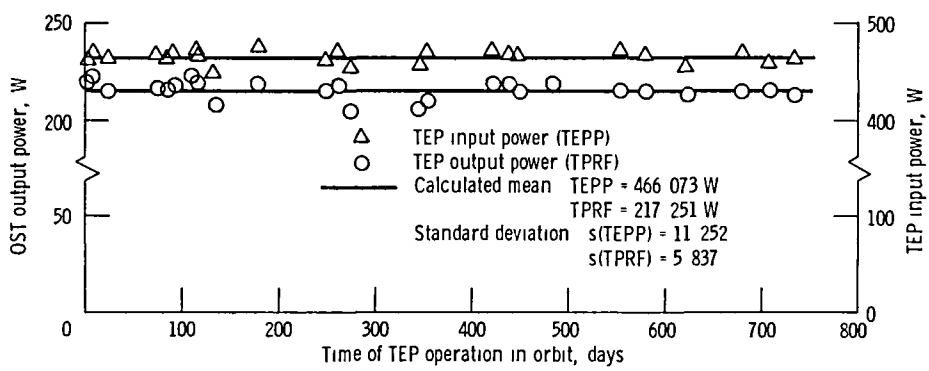

Figure 7 - OST input and output power at saturated output, center band

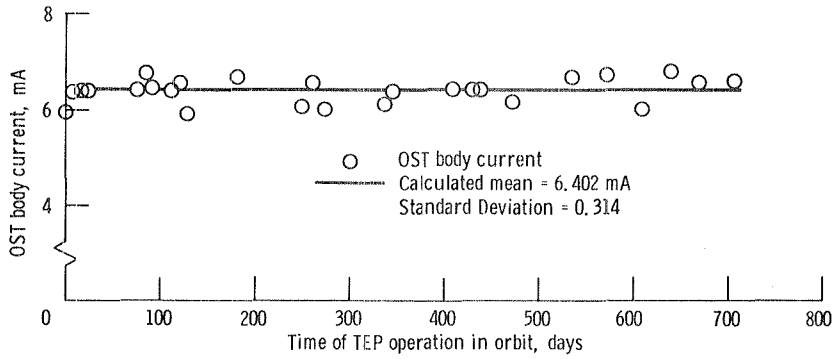

Figure 8. - OST body current at saturated output, center band.

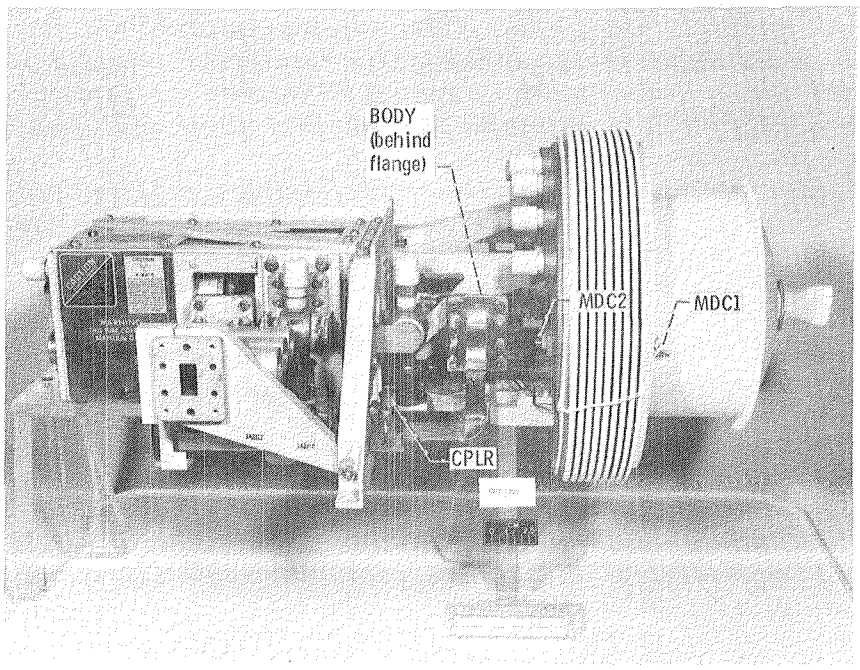

Figure 9. - Output stage tube, showing thermal instrumentation.

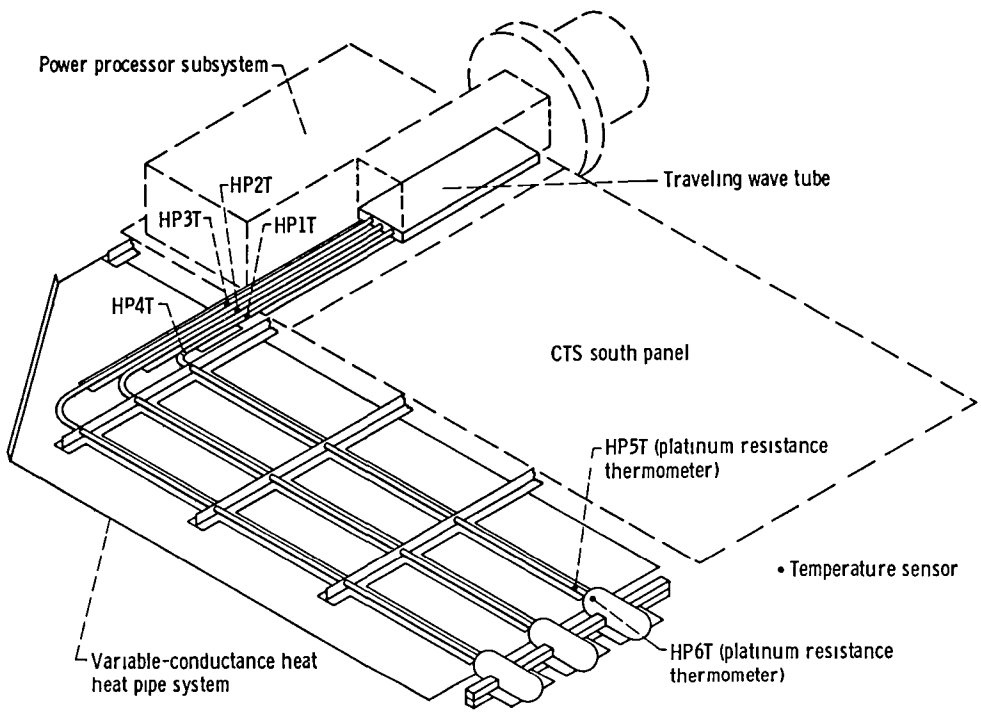

Figure 10 - Schematic of variable-conductance heat-pipe subsystem showing temperature sensor locations

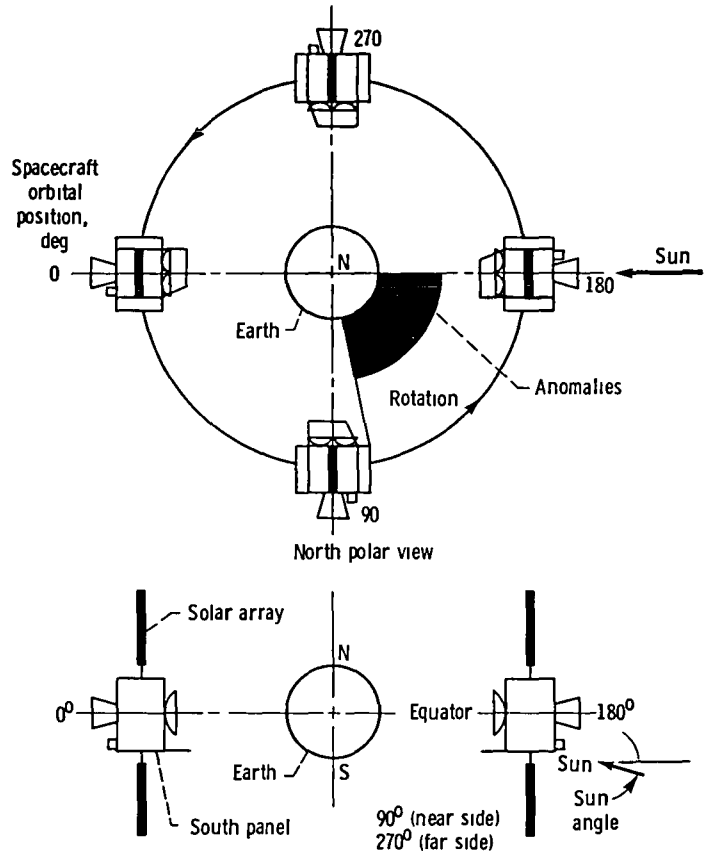

Figure 11 - CTS spacecraft orbital positions.

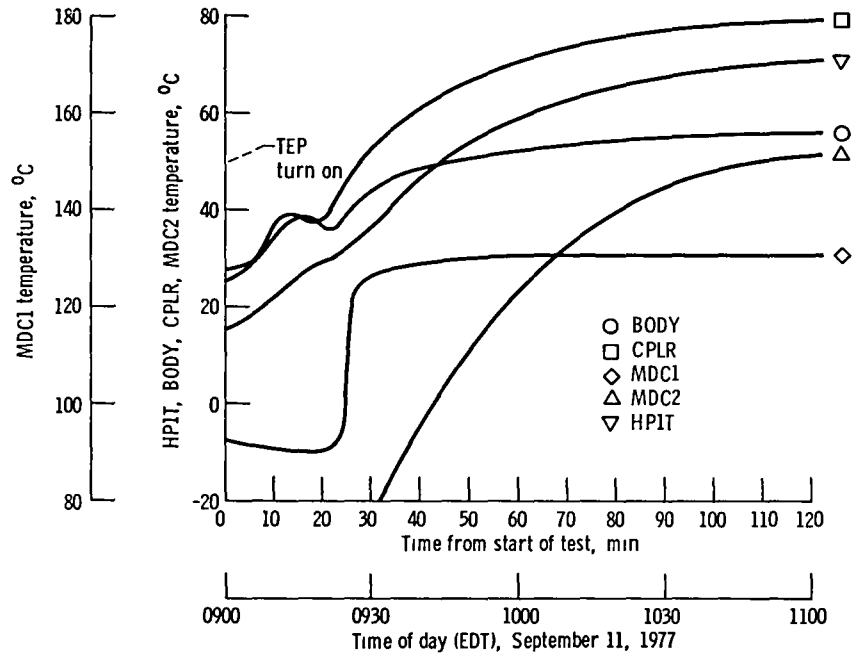

Figure 12 - Several output-stage-tube and variable-conductance heat pipe system temperatures during an output-stage thermal transient as functions of time Body current, 6 7 mA

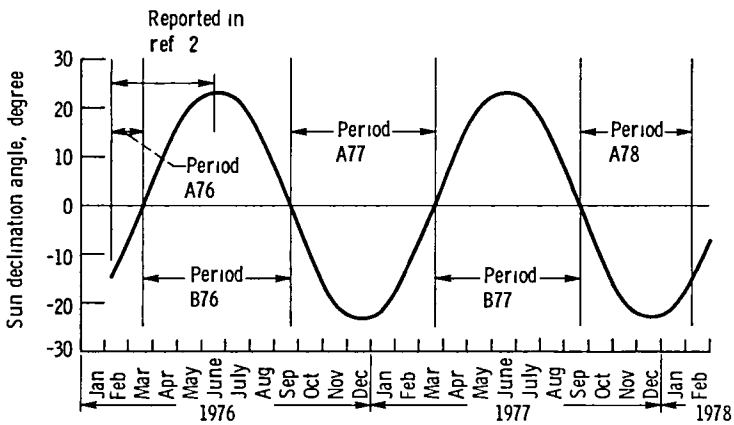

Figure 13 - Sun angle relative to equatorial plane (declination angle) at CTS spacecraft noon position (180^{o} orbital position) as function of date

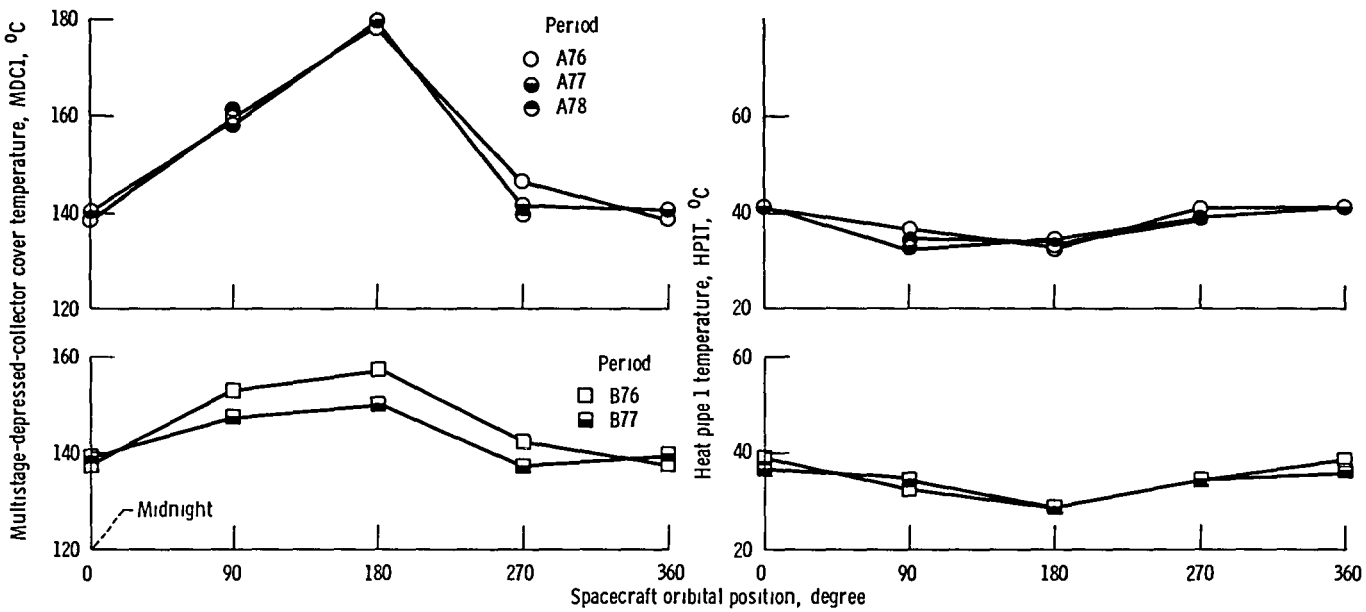

(a) Multistage-depressed-collector cover temperature

(b) Approximate output-stage-tube baseplate temperature

Figure 14 - TEP temperatures as a function of operating period and spacecraft orbit position operating conditions saturated rf output power, center band frequency (12 080 GHz)

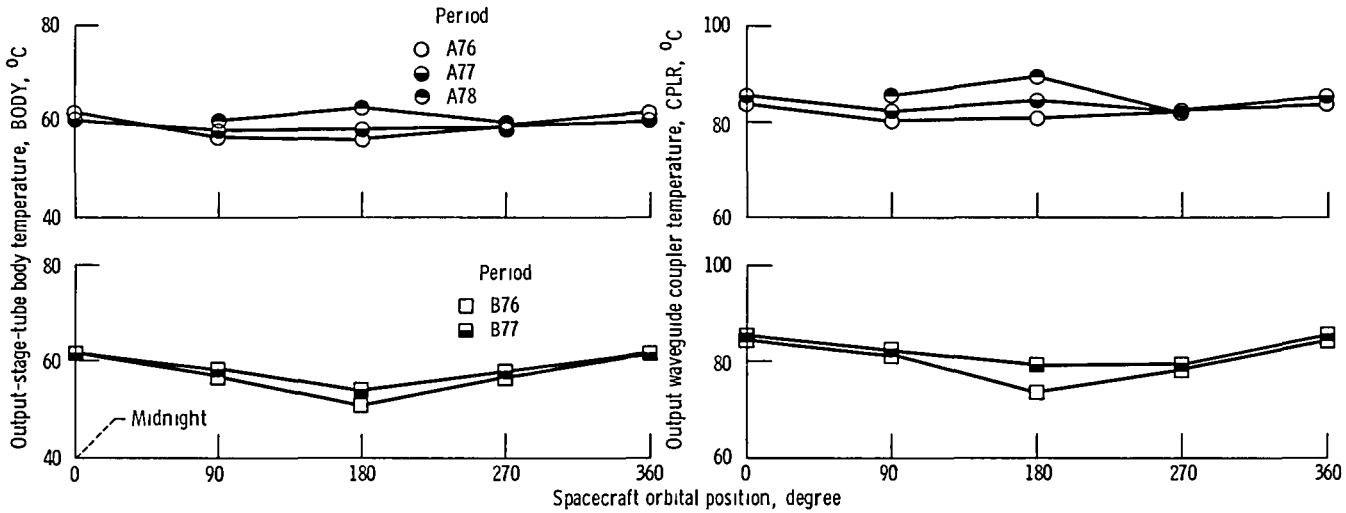

(c) Output-stage-tube body temperature

(d) Output waveguide coupler temperature

Figure 14 - Continued

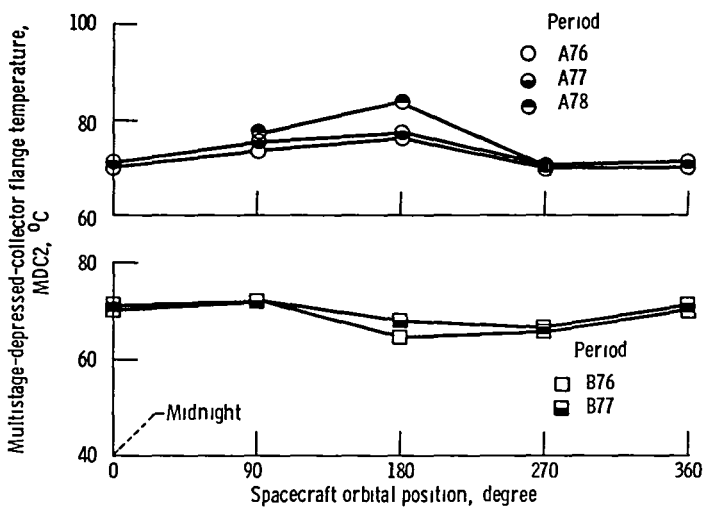

(e) Multistage-depressed-collector flange temperature

Figure 14 - Concluded

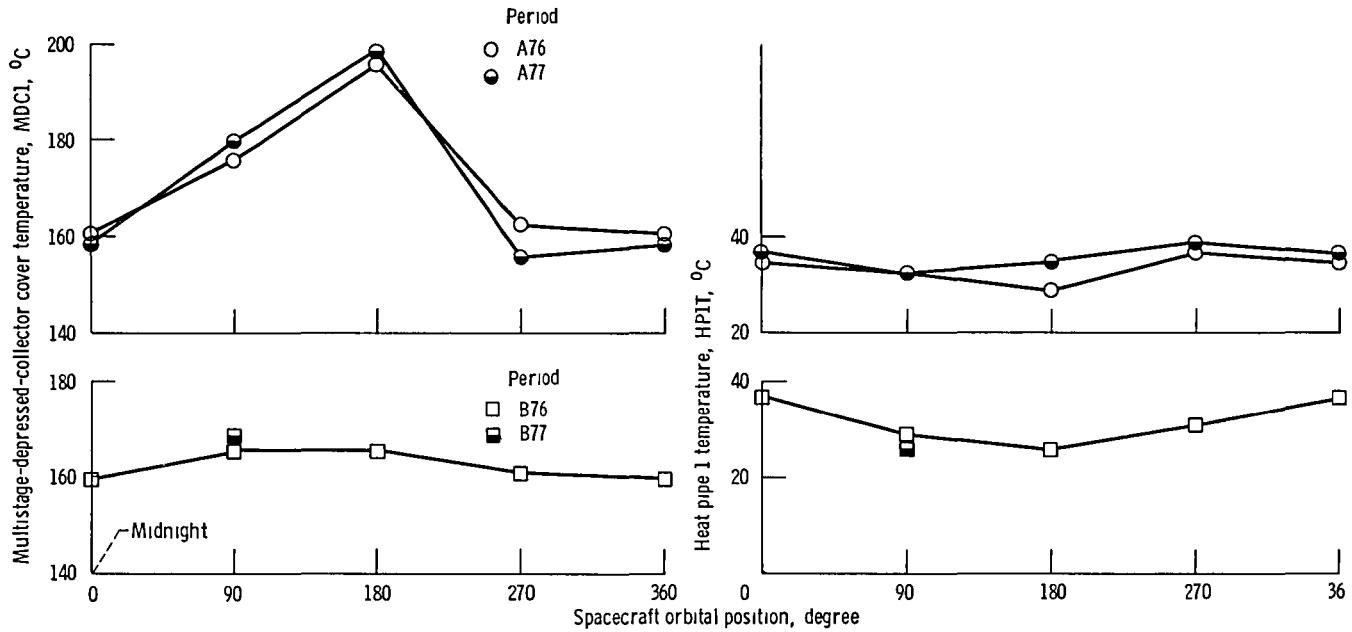

(a) Multistage-depressed-collector cover temperature.

(b) Approximate output-stage-tube baseplate temperature

Figure 15 - TEP temperatures as a function of operating period and spacecraft orbit position Operating conditions 100 W rf output power, center band frequency (12 080 GHz)

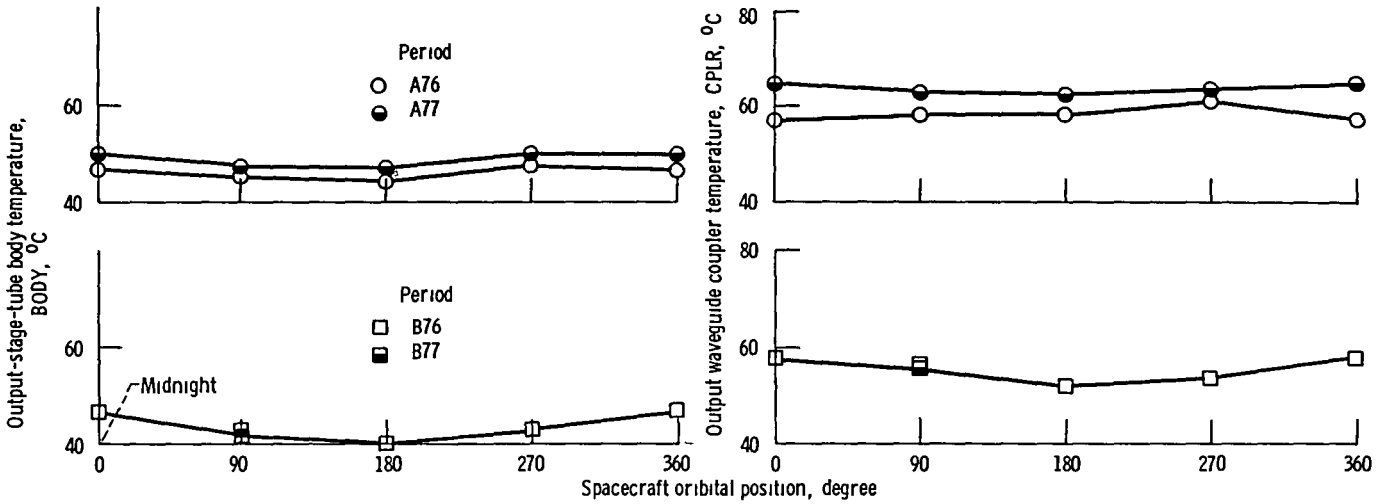

(c) Output-stage-tube body temperature

(d) Output waveguide coupler temperature

Figure 15 - Continued

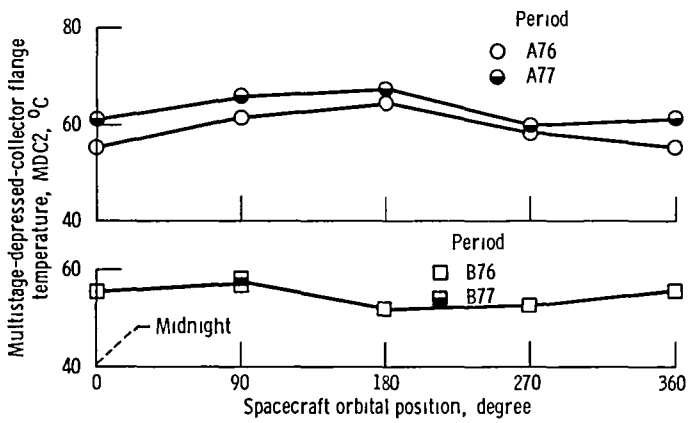

(e) Multistage-depressed-collector flange temperature

Figure 15 - Concluded

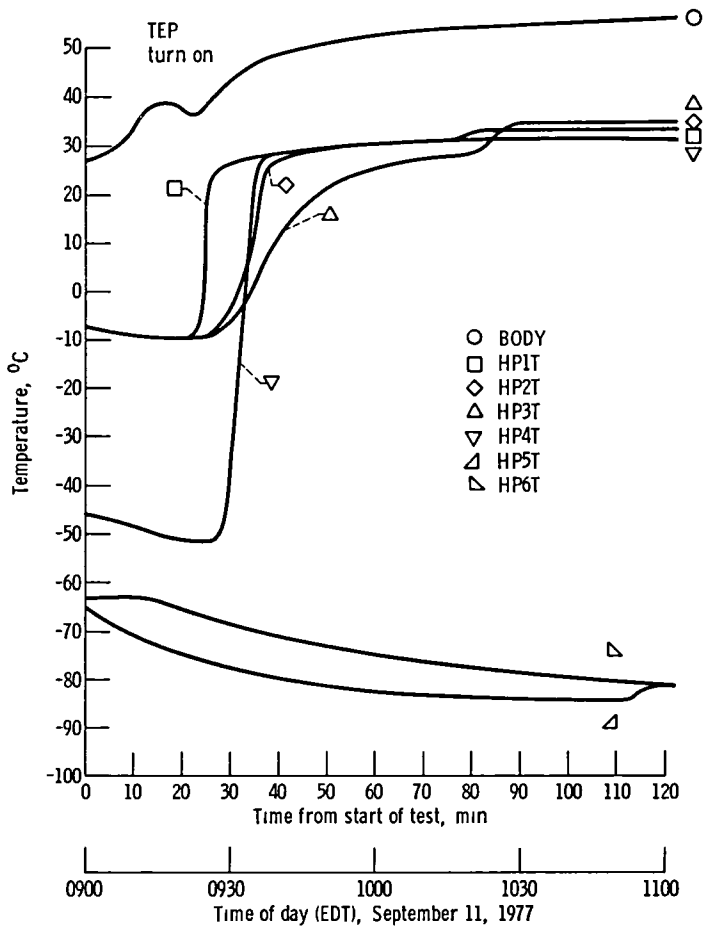

Figure 16 - Output-stage-tube body and variable-conductance heat pipe system temperatures as function of time

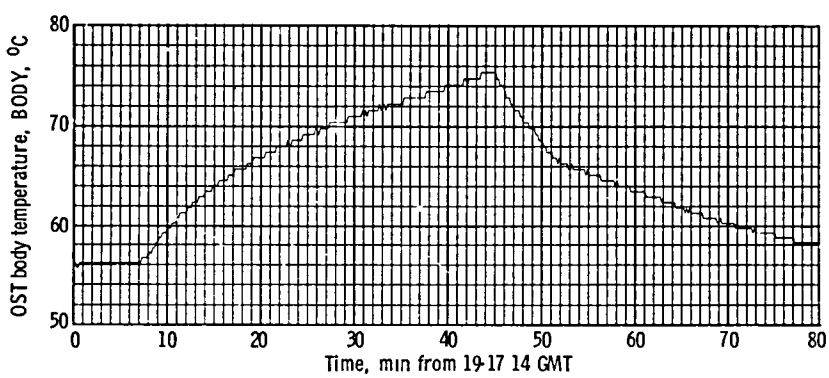

Figure 17. - OST body temperature response during TEP thermal anomaly period of day 75, 1977

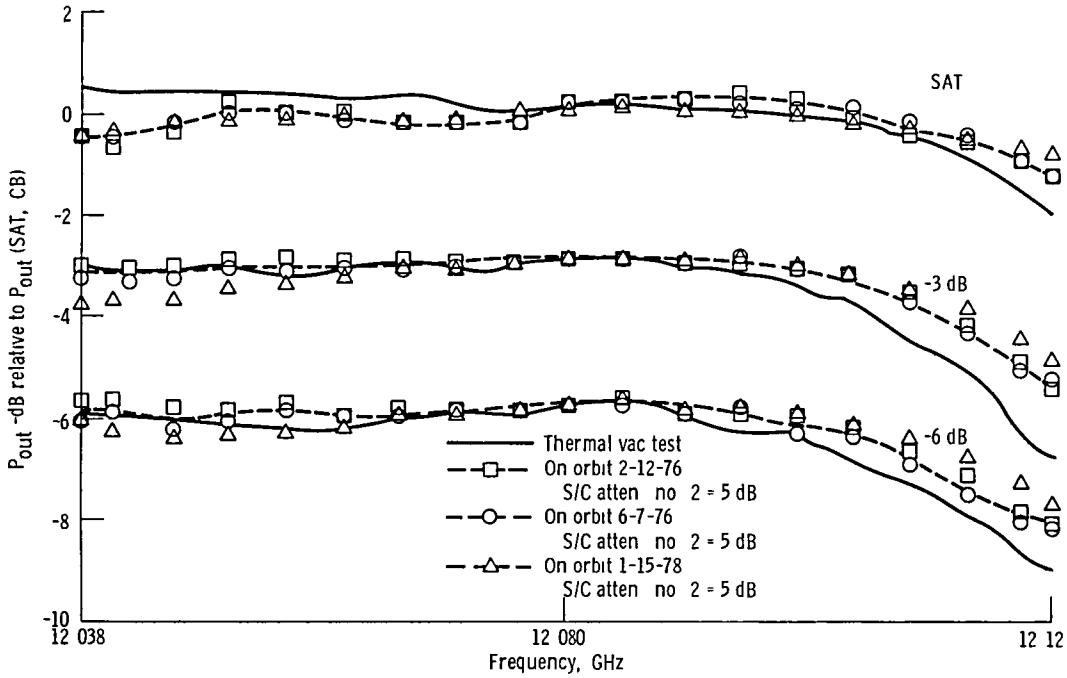

Figure 18 - Frequency response test

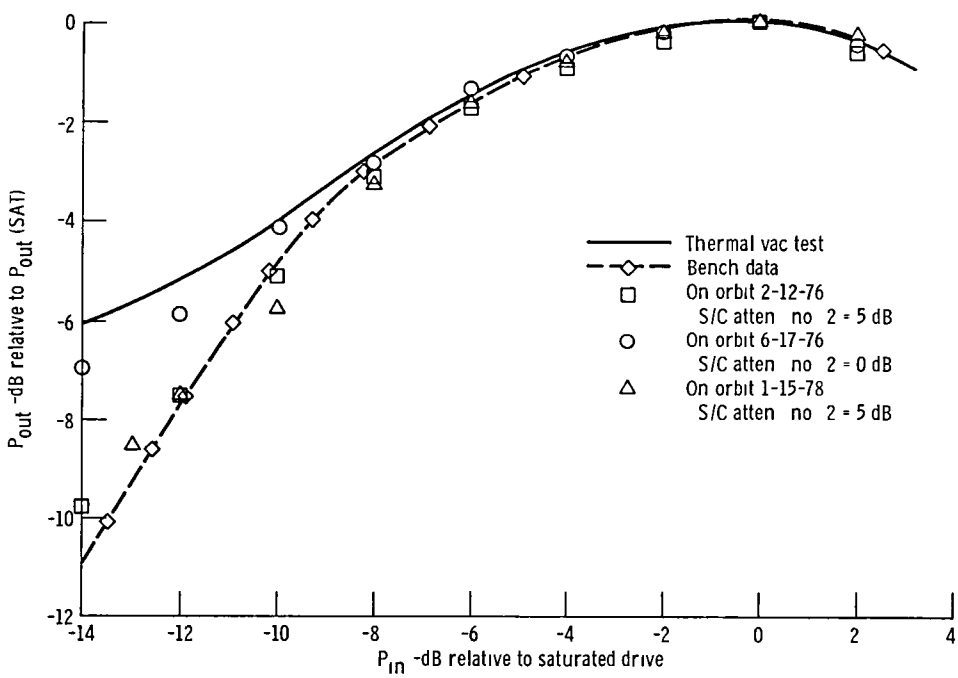

Figure 19 - P_{out} vs P_{in} test

1 Report No	2 Government Accession No	3 Recipient's Catalog No
NASA TM-79181		

4 Title and Subtitle	5 Report Date
LIFE CHARACTERISTICS ASSESSMENT OF THE COMMUNICATIONS TECHNOLOGY SATELLITE TRANSMITTER EXPERIMENT PACKAGE	July 1979
	6 Performing Organization Code

7 Author(s)	8 Performing Organization Report No
Jerry Smetana and Arthur N. Curren	E-049
	10 Work Unit No

9 Performing Organization Name and Address	11 Contract or Grant No
National Aeronautics and Space Administration Lewis Research Center Cleveland, Ohio 44135	

12 Sponsoring Agency Name and Address	13 Type of Report and Period Covered
National Aeronautics and Space Administration Washington, D.C. 20546	Technical Memorandum
	14 Sponsoring Agency Code

15 Supplementary Notes

16 Abstract

The performance characteristics of the transmitter experiment package (TEP) aboard the Communications Technology Satellite (CTS) measured during its first 2 years in orbit are presented in this report. The TEP consists of a nominal 200-watt output stage tube (OST), a supporting power processing system (PPS), and a variable-conductance heat pipe system (VCHPS). The OST, a traveling-wave tube augmented with a 10-stage depressed collector, has an overall saturated average efficiency of 51.5 percent and an average saturated radio-frequency (rf) output power at center-band frequency of 240 watts. The PPS operated with a measured efficiency of 86.5 to 88.5 percent. The VCHPS, using three pipes to conduct heat from the PPS and the body of the OST to a 52- by 124-centimeter (20.5- by 48.75-in.) radiator fin, maintained the PPS baseplate temperature below 50° C for all operating conditions. The TEP performance characteristics presented include frequency response, rf output power, thermal performance, and efficiency. Communications characteristics were evaluated by using both video and audio modulated signals. On four occasions, the TEP experienced temporary thermal control system malfunctions. While each of the anomalies was terminated safely, an investigation of the problem was conducted because of the potential for TEP damage due to the significant temperature increases associated with the anomalies. The investigation revealed the probable cause of the anomalies and safe TEP operating procedures have been established and are being observed.

17 Key Words (Suggested by Author(s))	18 Distribution Statement
Communications technology satellite Traveling wave tube Variable conductance heat pipe	Unclassified - unlimited STAR Category 17

19 Security Classif (of this report)	20 Security Classif (of this page)	21 No of Pages	22 Price*
Unclassified	Unclassified		

* For sale by the National Technical Information Service, Springfield Virginia 22161

End of Document